AD-A151 737 MATERIAL RESPONSE MODELS AND GROUND MOTION CALCULATIONS 1/1
FOR HIGH EXPLOSIV..(U) PACIFICA TECHNOLOGY DEL MAR CA
D PATCH ET AL. 25 JAN 84 PT-U83-0636 DNA-TR-84-124
UNCLASSIFIED DNA001-83-C-0058 F/G 19/4 NL

END
FILMED
DTIC

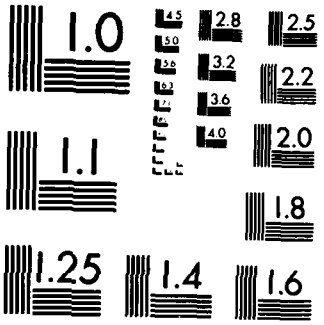

(2)

DNA-TR-84-124

# MATERIAL RESPONSE MODELS AND GROUND MOTION CALCULATIONS FOR HIGH EXPLOSIVE TESTS IN G-TUNNEL TUFF

Martin Fogel
Dan Patch
Pacifica Technology
P.O. Box 148
Del Mar, California 92014

25 January 1984

Technical Report

CONTRACT No. DNA 001-83-C-0058





THIS WORK WAS SPONSORED BY THE DEFENSE NUCLEAR AGENCY
UNDER RDT&E RMSS CODE C400083466 J24AMXJR00056 H2590D.



Prepared for
Director
DEFENSE NUCLEAR AGENCY
Washington, DC 20305

UNCLASSIFIED

SECURITY CLASSIFICATION OF THIS PAGE (When Data Entered)

| REPORT DOCUMENTATION PAGE | | READ INSTRUCTIONS BEFORE COMPLETING FORM |
|---|---|---|
| 1. REPORT NUMBER<br>DNA-TR-84-124 | 2. GOVT ACCESSION NO.<br>AD-A151737 | 3. RECIPIENT'S CATALOG NUMBER |
| 4. TITLE (and Subtitle)<br>MATERIAL RESPONSE MODELS AND GROUND MOTION CALCULATIONS FOR HIGH EXPLOSIVE TESTS IN G-TUNNEL TUFF | | 5. TYPE OF REPORT & PERIOD COVERED<br>Technical Report<br>6. PERFORMING ORG. REPORT NUMBER<br>PT-U83-0636 |
| 7. AUTHOR(s)<br>Dan Patch<br>Martin Fogel | | 8. CONTRACT OR GRANT NUMBER(s)<br>DNA 001-83-C-0058 |
| 9. PERFORMING ORGANIZATION NAME AND ADDRESS<br>Pacifica Technology<br>P. O. Box 148<br>Del Mar, California 92014 | | 10. PROGRAM ELEMENT, PROJECT, TASK AREA & WORK UNIT NUMBERS<br>Task J24AMXJR-00056 |
| 11. CONTROLLING OFFICE NAME AND ADDRESS<br>Director<br>Defense Nuclear Agency<br>Washington, DC 20305-1000 | | 12. REPORT DATE<br>25 January 1984<br>13. NUMBER OF PAGES<br>80 |
| 14. MONITORING AGENCY NAME & ADDRESS(if different from Controlling Office)<br>Commander<br>Field Command/Defense Nuclear Agency<br>Kirtland AFB, NM 87117 | | 15. SECURITY CLASS. (of this report)<br>UNCLASSIFIED<br>15a. DECLASSIFICATION/DOWNGRADING SCHEDULE<br>N/A since Unclassified |

16. DISTRIBUTION STATEMENT (of this Report)

Approved for public release; distribution is unlimited.

17. DISTRIBUTION STATEMENT (of the abstract entered in Block 20, if different from Report)

18. SUPPLEMENTARY NOTES

This work was sponsored by the Defense Nuclear Agency under RDT&E RMSS Code C400083466 J24AMXJR00056 H2590D.

19. KEY WORDS (Continue on reverse side if necessary and identify by block number)

Material Response
Constitutive Models
Ground Motion
Tuff
Shock Damage
Dilatation
Viscoelastic

20. ABSTRACT (Continue on reverse side if necessary and identify by block number)

Numerical material response models developed from static laboratory material response measurements and from dynamic explosive test data are described. Material models were first specified using only laboratory test data obtained by Terra Tek. Predictions using this model were then compared to dynamic stress and velocity data taken by SRI International in very small (3/8 gm PETN) explosive shots, and by Sandia Laboratories in a much larger scale (2000 lb. TNT) ONE-TON test. All laboratory measurements and SRI shots used tuff samples taken from the Sandia ONE-TON test site located in G-Tunnel at the Nevada Test Site. A new

DD FORM 1 JAN 73 1473 EDITION OF 1 NOV 65 IS OBSOLETE
S/N 0102-LF-014-6601

UNCLASSIFIED

SECURITY CLASSIFICATION OF THIS PAGE (When Data Entered)

20. ABSTRACT (Continued)

material model was constructed to agree as closely as possible with the SRI data and a second prediction for the ONE-TON event was made.

Overall the ONE-TON predictions were quite good if the expected bias in air-void content was considered, with the model using the SRI results doing slightly better. The comparisons highlighted concerns about the measured air-void content and uncertainties in the strain rate dependence of material properties. Models including dilatation and viscoelastic effects were developed and predictions from these models are compared with the test data. The viscoelastic model was quite successful at both the SRI and ONE-TON scale. The dilatation model had some encouraging features but requires additional data and development.

## TABLE OF CONTENTS


| Section | | Page |
|---|---|---|
| 1. | INTRODUCTION AND SUMMARY | 7 |
| 2. | MATERIAL RESPONSE MODELS | 10 |
| 2.1 | Introduction | 10 |
| 2.2 | Physical Properties | 11 |
| 2.3 | Porous Crush Response | 13 |
| 2.4 | Shear Modulus Model | 21 |
| 2.5 | Virgin and Damaged Yield Strength Models | 31 |
| 2.6 | Viscoelastic Model | 35 |
| 2.7 | Dilatation Response | 37 |
| 2.8 | Calculational Geometry and Procedure | 39 |
| 3. | COMPARISON WITH SRI VELOCITY HISTORIES | 44 |
| 4. | COMPARISON WITH ONE-TON TEST DATA | 56 |
| 5. | SUMMARY AND CONCLUSIONS | 71 |
| | REFERENCES | 75 |


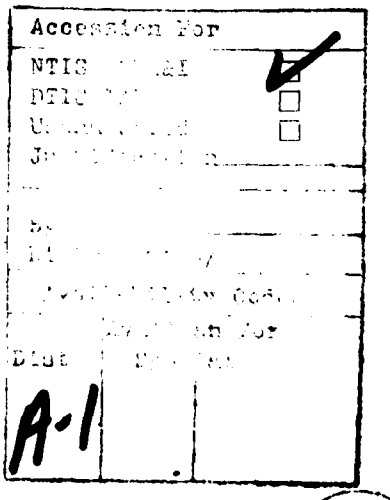

## LIST OF ILLUSTRATIONS


Figure — Page

1. Typical p-v response mesured by Terra Tek on U12G-OT core showing fit parameters summarized in Tables 3 and 4 . . . . . 15

2. Porous crush response in older G-Tunnel tuff calculations and this study . . . . . 20

3. Representative uniaxial load-unload response by Terra Tek on virgin U12G-OT core samples and damaged triaxial response . . . . . 22

4. Effective shear modulus measured from uniaxial unloading response of U12G-OT tuff. . . . . 26

5. Cycled uniaxial test data by Terra Tek showing hysteresis in the unloading-reloading response . . . . . 27

6. Numerical model uniaxial test, cycled response . . . . . 29

7. Comparison of calculated G-Tunnel tuff response with Terra Tek data for a uniaxial load, uniaxial unload, biaxial unload test sequence . . . . . 30

8. Typical uniaxial load, biaxial unload, triaxial reloading response measured by Terra Tek for U12G-OT tuff . . . . . 33

9. Sketch of hypothetical yield surface illustrating generalized associated flow rule adopted in dilatation calculations . . . . . 38

10. Calculated p-v load-unload response with dilatation model . . . . . 40

11. Calculated stress difference vs. confining stress curves with dilatation model . . . . . 41

12. Typical Terra Tek U12G-OT tuff uniaxial load, biaxial unload, triaxial loading data corresponding to the stress difference data shown in Figure 8. . . . . 42

13. Comparison of SRI experiment data and calculation at 1.90 cm location. . . . . 45

14. Comparison of SRI experiment data with calculation using 2.2% air-void content and strain rate hardening on all the time . . . . . 47

## LIST OF ILLUSTRATIONS (Continued)


Figure — Page

15. Comparison of SRI experiment data with calculation using 2.2% air-void content and strain rate hardening on all the time ..... 48

16. Comparison of SRI experiment data with a calculation using 0.69% air-void content ..... 49

17. Comparison of SRI experiment data with a calculation using 0.69% ..... 50

18. Comparison of SRI experiment data with a calculation using a viscoelastic model and no air-void content ..... 52

19. Comparison of SRI experiment data with a calculation using a viscoelastic model an no air-void content ..... 53

20. Volumetric strain measured by SRI by differencing particle velocity traces obtained in SNLA G-Tunnel tuff ..... 54

21. Comparison of ONE-TON data with a calculation using the baseline static model with 0.69% air-void content ..... 57

22. Comparison of ONE-TON data with a calculation using the baseline static model with 0.69% air-void content ..... 58

23. Comparison of ONE-TON data with a calculation using the baseline static model with 0.69% air-void content ..... 59

24. Comparison of ONE-TON data with a calculation using the baseline static model with 0.69% air-void content ..... 60

25. Comparison of ONE-TON data with a calculation using the baseline static model with 0.69% air-void content and strain rate hardening on after damage ..... 61

26. Comparison of ONE-TON data with a calculation using the baseline static model with 0.69% air-void content and strain rate hardening on after damage ..... 62

27. Comparison of ONE-TON data with a calculation using the viscoelastic model ..... 64

28. Comparison of ONE-TON data with a calculation using the viscoelastic model ..... 65

29. Comparison of ONE-TON data with a calculation using the viscoelastic model ..... 66

## LIST OF ILLUSTRATIONS (Concluded)


Figure | Page

30. Comparison of ONE-TON data with a calculation using the viscoelastic model ..... 67

31. Comparison of ONE-TON data with a calculation using a model with 2.2% air-void content and dilatancy ..... 68

32. Comparison of ONE-TON data with a calculation using a model with 2.2% air-void content and dilatancy ..... 69

## LIST OF TABLES


| Table | | Page |
|---|---|---|
| 1. | Average physical properties from tuff core samples taken in drill holes U12N.12, U12N.15, U12N.18 and U12G-OT | 12 |
| 2. | Calculated physical properties and ultrasonic moduli for tuff samples taken in U12N.12, U12N.15, U12N.18 and U12G-OT | 14 |
| 3. | Summary of unloading compressibility data for U12G-OT tuff derived from the slope of p-v curves obtained in uniaxial strain to 1, 2, and 4 kbar | 16 |
| 4. | Summary of p-v comparison data measured by Terra Tek in uniaxial strain tests on tuff samples from the U12G-OT-IH#1 and IH#2 drill holes. | 17 |
| 5. | Effective moduli and Poisson's ratio measured from the unloading portion of uniaxial strain tests conducted by Terra Tek on core samples taken form the U12G-OT-IH#1 and IH#2 drill holes | 23 |
| 6. | Effective shear modulus parameters used to model the response of G-Tunnel tuff | 28 |

## SECTION 1
## INTRODUCTION AND SUMMARY

Numerical calculations are often used to help in the design of a containment plan by evaluating the risk of failure due to particular features of the plan. Variations in geometry and material properties are more readily studied numerically than in full scale field tests. Reliability and the predictive capability of the calculations are the central issues that must be confronted when using numerical results as input to design decisions. The computations are not self contained. They require models that can faithfully specify the response of all the materials in the problem throughout the entire stress-strain regime of interest. The greatest uncertainty lies in the equation of state modeling, consequently, any program that helps in improving and validating these models increases confidence in the calculations. This report discusses a series of comparisons between two experiments and a corresponding suite of calculations whose main goal was to focus on the adequacy of equation of state models used in the majority of our containment calculations.

The experimental part of the procedure used to test the current models centered on data from the ONE-TON test, a high explosive event using a 2000 pound TNT charge that was fired by Sandia in G-Tunnel.[1] Cores from the ONE-TON working point (WP) were sent to Terra Tek for a complete set of material properties tests. In addition to the usual physical property and uniaxial load tests, the ONE-TON tuff was subjected to a variety of special, uniaxial load-biaxial unload and multi-cycle, load-unload tests.[2] These tests provided a comprehensive and detailed picture of the static response of this tuff. In addition to the data from the Sandia ONE-TON event, a family of velocity time histories was recorded by SRI International from laboratory scale HE tests using a 3/8 gm PETN charge detonated in a core of this G-Tunnel tuff.[3] As discussed below, the SRI data contributed to the definition of the dynamic response of the tuff.

A series of calculations was performed here at PacTech in concert with the Sandia and SRI experiments. Using only the static material test data gathered by Terra Tek, a material model was constucted and predictions for the SRI and ONE-TON tests were made. The predictions for the SRI experiment were compared with the results of the test, and a new model was constucted to agree as closely as possible with the

experiment. This model was then used to produce a second prediction for the ONE-TON event. Finally, a comparison was made between the two predictions and the results of the ONE-TON test.

Such a series of comparisons focus sharply on the adequacy of the material modeling. Test site complications are minimized since the test geometries are relatively small scale, simple spherical explosions in a fairly homogeneous tuff. The ONE-TON comparisons are particularly relevant in that both stress and velocity histories were obtained, and the scale of this test is closer to that of a nuclear event than are laboratory size SRI tests with their 3/8 gm charge. The rather unique circumstance of having both static material response data and dynamic ground motion data from two different small scale tests, focuses on the issue of the minimal suite of static and dynamic laboratory tests required to define a material model that will faithfully reproduce the response in a full scale test.

The comparisons provided some interesting insight. Overall, both of the ONE-TON predictions did quite well, with the model based on the SRI test doing slightly better. The comparisons highlighted two issues concerning the modeling process, the air-void content and strain rate dependence of material properties.

The best agreement between calculation and experiment was obtained with an air-void content considerably below that measured in uniaxial crush tests. This had been noticed in earlier calculations for a variety of tests, such as RS-15, done in G-Tunnel. This issue is further clouded by the presence of dilatant behavior measured statically by Terra Tek and dynamically by SRI. Reconciling the statically measured air-void content with the dynamic response remains an area requiring further study.

The second problem posed by the experiments is the seeming lack of scale invariance between the 3/8 gm and ONE-TON shots. The presence of strain rate effects makes it very difficult to extrapolate material properties over a large range in rate. The relevance of data taken at any rate scale depends on the degree of importance of the rate effects and an understanding of them. In part, the usefulness of the small scale SRI experiments is to point out the presence of strain rate effects by going to a very extreme rate. A knowledge of the nature of the strain rate effect is required in order to

use either the lab data or the SRI data to build a model that is reliable at the ultimate scale of interest.

Section 2 contains a discussion of the constuction of an equation of state for G-Tunnel tuff based on the static tests done by Terra Tek. The predictions for the SRI scale test are compared with the data in Section 3. The agreement was not very good, and a model that fits the SRI results was constructed. A comparison using this new model demonstrates the degree of agreement obtained. Predictions of the ONE-TON event using these models are compared with the experimental results in Section 4. A summary of the conclusions reached and the questions raised by this study are contained in Section 5.

# SECTION 2
# MATERIAL RESPONSE MODELS

## 2.1 INTRODUCTION

Construction of the various equation of state (EOS) and constitutive response models for the ONE-TON, G-Tunnel tuff is discussed in this section. A variety of material response tests and physical property measurements obtained in the laboratory by Terra Tek[2] served as the primary source of data for this model building process; however, recent data from Terra Tek tests in tuffs other than the ONE-TON tuff[4] provided additional input into the model. Finally, it should be noted that not all of the ONE-TON tuff response data was available during the course of the calculational program. Indeed, one of the most important findings of this work was the need for a clearer definition of several features of the tuff behavior (e.g., dilation, strength degradation, and in situ air-void content). These questions are being actively pursued, and significant new data have already been reported.[5]

As discussed in Section 1, a central objective of this research was to focus on the adequacy of current material models as developed from static response test data. As a consequence, unusual care was taken to reproduce all aspects of the tuff behavior with as much fidelity as possible. Some deviations from the observed response were required, as will be discussed.

The constitutive model consists of a number of parts that will be treated in turn. Physical property measurements describe the composition of the tuff in terms of its mineral, water and air-void content, sonic velocities, and densities (ambient, dry and grain). Compressive tests, either hydrostatic, uniaxial, or biaxial, provide information on the bulk compressibility of the tuff, both with and without air-void inclusions. Although the pressure-volume (p-v) response of earthen materials can be a function of both the deviatoric and the mean normal stress (pressure) paths (as well as strain in the case of a dilating material), the numerical p-v response models generally are couched only in terms of the pressure component of the stress state since the deviatoric contribution is small and difficult to identify with any certainty. The deviatoric response of the tuff is separated into elastic and perfectly plastic stress-strain regimes. Behavior in the elastic

Table 5. (Continued)

| HOLE | DEPTH | MAXIMUM CONFINING STRESS (kbar) | PRESSURE (kbar) | SLOPE | BULK MODULUS (kbar) | POISSON'S RATIO | SHEAR MODULUS (kbar) |
|---|---|---|---|---|---|---|---|
| IH#1 | 14.0-14.5 | 1 | 0.5 | 0.3200 | 100 | 0.4310 | 14.46 |
| " | " | " | 1 | 0.5128 | 133 | 0.3980 | 29.12 |
| IH#1 | 56.3-57.8 | 1 | 0.5 | 0.3700 | 95 | 0.4219 | 15.65 |
| " | " | " | 1 | 0.5479 | 120 | 0.3925 | 27.80 |
| IH#1 | 54.8-56.3 | 1 | 0.5 | 0.2800 | 120 | 0.4386 | 15.37 |
| " | " | " | 1 | 0.4598 | 120 | 0.4065 | 23.92 |
| IH#1 | 18.8-19.5 | 0.5 | 0.5 | 0.4878 | 93 | 0.4020 | 19.51 |
| IH#1 | 54.8-56.3 | 0.5 | 0.5 | 0.5000 | 120 | 0.4000 | 25.71 |

Table 5. Effective moduli and Poisson's ratio measured from the unloading portion of uniaxial strain tests conducted by Terra Tek on core samples taken from the U12G-OT-IH#1 and IH#2 drill holes.

| HOLE | DEPTH | MAXIMUM CONFINING STRESS (kbar) | PRESSURE (kbar) | SLOPE | BULK MODULUS (kbar) | POISSON'S RATIO | SHEAR MODULUS (kbar) |
|---|---|---|---|---|---|---|---|
| IH#1 | 53.2-55.0 | 4 | 2 | 0.1250 | 132 | 0.4706 | 7.92 |
| " | " | " | 3 | 0.2667 | 175 | 0.4412 | 21.43 |
| " | " | " | 4 | 0.4167 | 220 | 0.4138 | 40.24 |
| IH#1 | 56.3-57.8 | 4 | 3 | 0.3500 | 155 | 0.4255 | 24.29 |
| " | " | " | 4 | 0.5333 | 225 | 0.3947 | 50.94 |
| IH#1 | 53.9-56.3 | 4 | 3 | 0.2125 | 165 | 0.4520 | 16.37 |
| " | " | " | 4 | 0.3000 | 225 | 0.4348 | 30.68 |
| IH#1 | 54.8-56.3 | 4 | 3 | 0.1750 | 150 | 0.4598 | 12.40 |
| " | " | " | 3.5 | 0.3000 | 170 | 0.4348 | 23.18 |
| " | " | " | 4 | 0.5161 | 175 | 0.3974 | 38.53 |
| IH#1 | 51.9-58.2 | 4 | 3 | 0.2250 | 150 | 0.4494 | 15.70 |
| " | " | " | 4 | 0.3750 | 175 | 0.4211 | 29.17 |
| IH#2 | 56.1-57.7 | 4 | 3 | 0.2000 | 170 | 0.4545 | 15.94 |
| " | " | " | 4 | 0.3500 | 225 | 0.4255 | 35.26 |
| IH#1 | 23.5-24.5 | 2 | 1 | 0.3000 | 131 | 0.4348 | 17.86 |
| " | " | " | 1.5 | 0.4545 | 140 | 0.4074 | 27.63 |
| " | " | " | 2 | 0.6452 | 160 | 0.3780 | 42.48 |
| IH#2 | 52.8-53.2 | 2 | 1 | 0.2125 | 130 | 0.4520 | 12.90 |
| " | " | " | 2 | 0.2500 | 185 | 0.4444 | 21.35 |
| IH#2 | 55.0-56.1 | 2 | 1 | 0.1250 | 125 | 0.4706 | 7.50 |
| " | " | " | 1.5 | 0.2250 | 145 | 0.4494 | 15.17 |
| " | " | " | 2 | 0.3833 | 145 | 0.4196 | 24.64 |
| IH#1 | 39.5-40.5 | 2 | 1 | 0.1800 | 115 | 0.4587 | 9.76 |
| " | " | " | 1.5 | 0.3750 | 128 | 0.4211 | 21.33 |
| " | " | " | 2 | 0.5882 | 135 | 0.3864 | 33.20 |
| IH#1 | 43.1-44.1 | 2 | 1 | 0.2000 | 125 | 0.4545 | 11.72 |
| " | " | " | 1.5 | 0.3000 | 125 | 0.4348 | 17.05 |
| " | " | " | 2 | 0.4878 | 130 | 0.4028 | 27.27 |

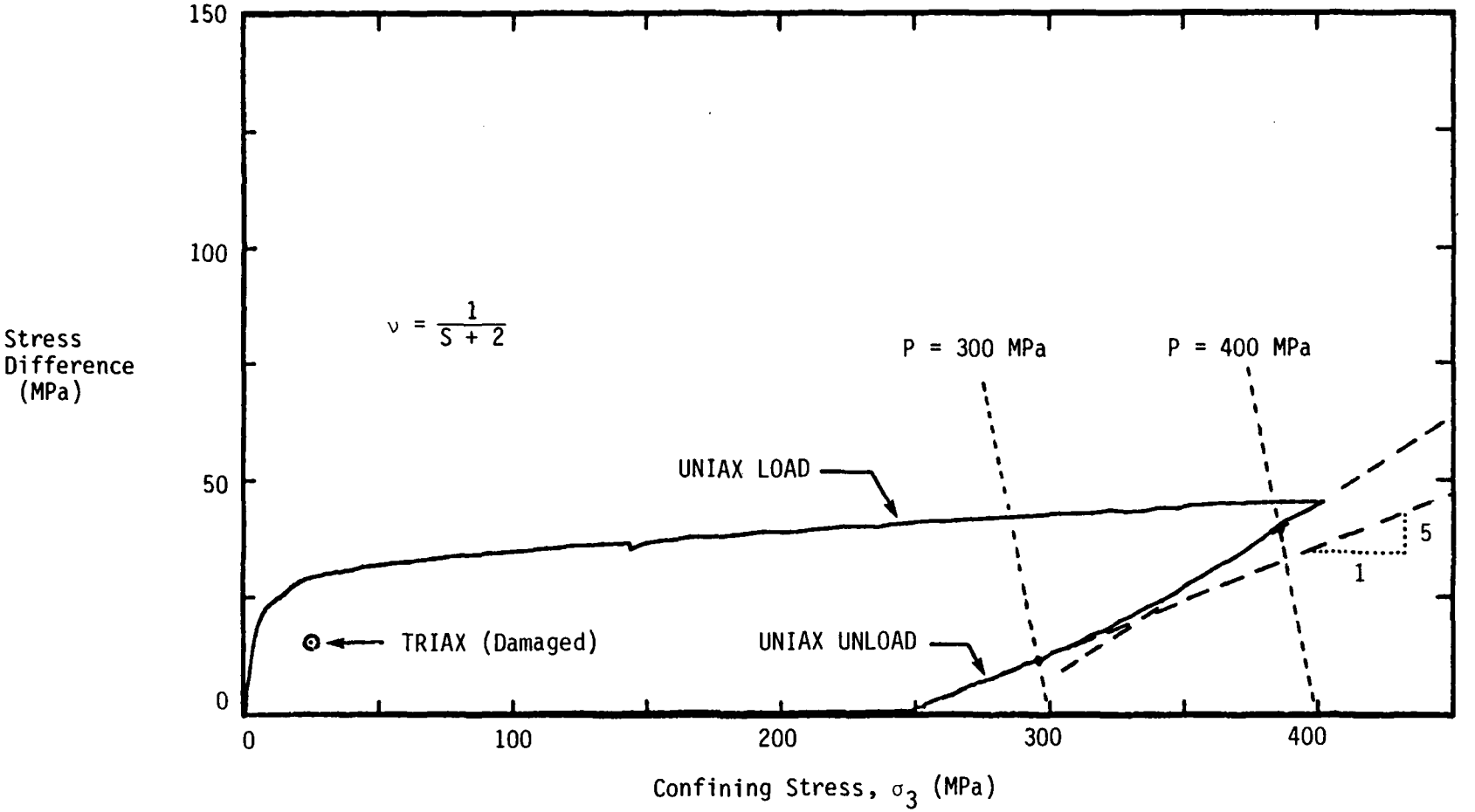


Figure 3. Representative uniaxial load-unload response measured by Terra Tek on virgin U12G-OT core samples and damaged triaxial response.

of ~10 MPa. At the outset of this study these older p-v data were reexamined. Three samples appeared to have very abnormally high compaction (ranging from 4.3 to 5.9%) while none of the "low" values seemed to be remarkably anomalous. Thus there appeared to be some justification for rejecting the three "high" air-void samples while retaining the remainder of the data. This procedure gave an average residual compaction above the 10 MPa base pressure of 0.69% and this value was assumed in the baseline model discussed in Section 3.

In contrast to N-Tunnel tuff for which 400 MPa is not an unusual crush pressure, all of the uniaxial load-unload test data for G-Tunnel tuff imply that complete compaction is achieved at relatively low levels of pressure (below 200 MPa). In an effort to preserve the observed static p-v response to the maximum extent possible, while still accommodating the reduced air-void content assumed in some of the calculations, the basic shape of the 2.195% air-void content crush curve was retained by scaling the volumetric response from the oringinal 2.19% air-void crush curve as illustrated in Figure 2.

## 2.4 SHEAR MODULUS MODEL

Effective values for Poisson's ratio on unloading can be computed from the Terra Tek uniaxial stress difference vs. confining stress curves (see Figure 3 and Table 5). Using the bulk modulus obtained from the p-v curve at the corresponding state then defines all of the other effective moduli. It is important to note that the material models contained in the codes treat deformations below the yield surface as purely elastic, while the true material deformation, at least on the microscale of the rock matrix, almost certainly is a very complex. Thus, to avoid the inference that the moduli correspond to a purely elastic process, they have been designated as "effective" moduli in Tables and the preceeding discussion. Nevertheless, on the macroscopic scale appropriate to the material tests and explosive shot data, the observed material response can be duplicated in the numerical model using a variable shear (and bulk) modulus formulation.

Although most of our previous ground motion calculations have used a constant shear modulus formulation, various variable shear modulus models have occasionally been

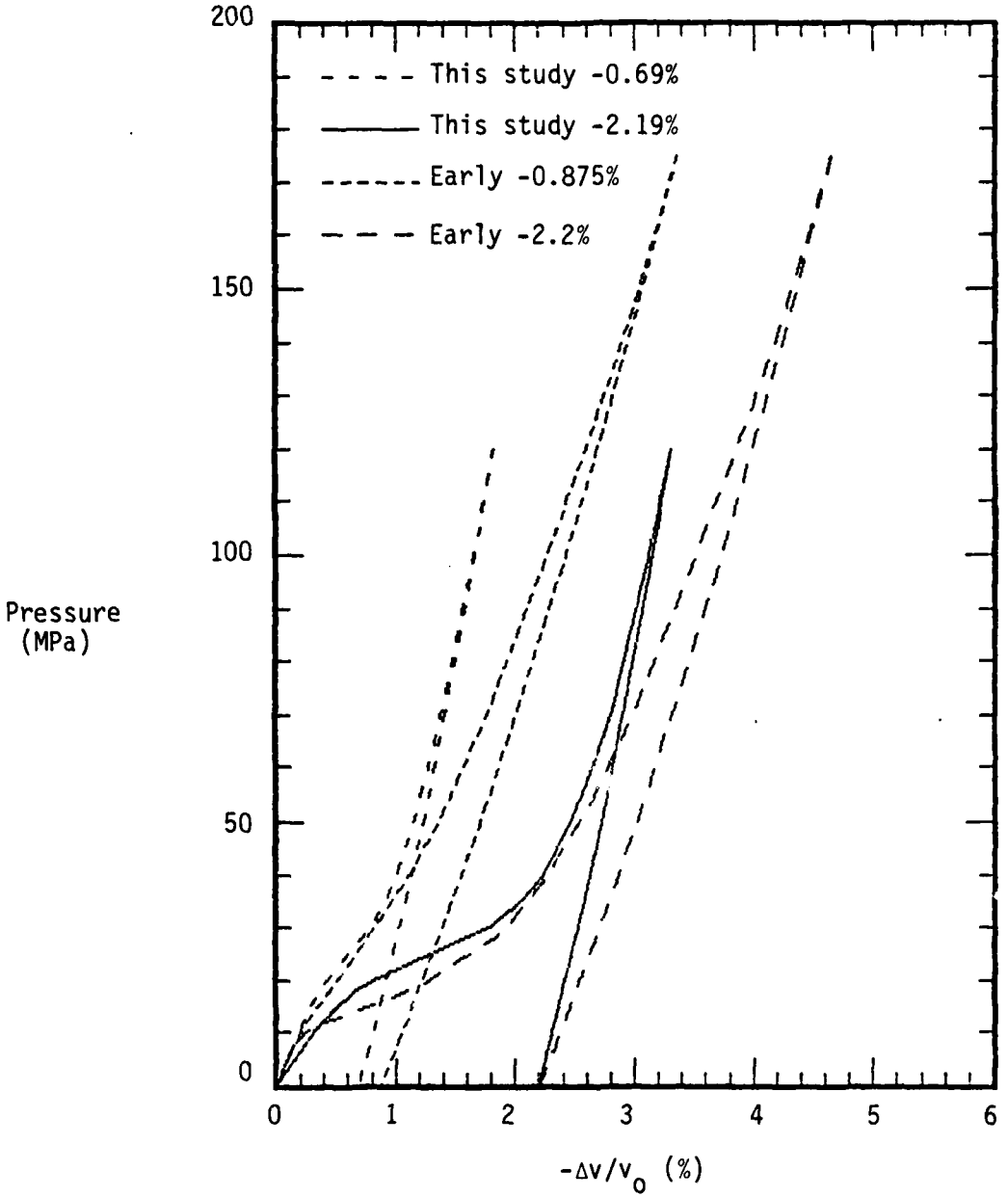


Figure 2. Porous crush response in older G-Tunnel tuff calculations and this study.

outset of the loading phase of the test. Little credence was attached to this portion of the curve, given the precision of the measurement and the likelihood that some of this behavior was attributable to end effects on the sample as the tuff seated in the test apparatus. This problem is much less pronounced in the Terra Tek ONE-TON data; nevertheless, it still creates some uncertainty regarding the true initial state of the tuff in situ. The steepest portion of the initial loading curve was taken to be a reasonable estimate of the true zero pressure bulk modulus of the material (see Figure 1 and Table 4). Additionally, in the explosive experiments the G-Tunnel tuff was preloaded by the in situ stress state which we took to be 5.96 (±0.40) MPa based on the in situ mean normal stress reported by Ellis and Ege in G-Tunnel at the ONE-TON shot depth[6]. Table 4 lists the combined contributions of the correction for the zero offset and the prestress to ~ 6.0 MPa. Figure 2 illustrates the shape of the p-v response used in the 2.19% air-void computations and compares this response with older G-Tunnel tuff models. The 2.19% air-void content value was chosen as the mean of the complete data set and the data set rejecting 'high' and 'low' values (see Table 4). Clearly, there is an uncertainty of about 0.2% in this 2.19% value for the static, insitu air-void content, depending on which data set is chosen. Whatever value is used, the correction to in situ conditions is significant (~ 0.28%) and the static test data are outside the statistical limits of uncertainty in comparison to the physical properties data (~1.40%, Table 1).

A number of earlier PacTech ground motion calculations have been made in support of various Sandia high explosive containment shots in G-Tunnel (e.g., the RS shot series and the DM low yield stemming design model tests)[7-9]. The material property data base for these calculations was quite limited as discussed in Reference 7. It is of interest to note that the measured average air-void content based on uniaxial compaction to 400 MPa for this old and limited data base was 2.2%, in substantial agreement with the recent U12G-OT measurements. An early finding of these original G-Tunnel studies was that the assumed air-void content of 2.2% considerably overestimated the in situ air-void content of the tuff as evidenced by calculated stress attenuation rates considerably higher than those observed in most of the Sandia tests (the DM-1 and DM-2 shot sites, however, were unusually dry). Subsequent G-Tunnel calculations used an air-void content of 0.875% derived from the existing data set (16 tests, not all at tunnel level) by rejecting the three highest and three lowest measured air-void values and then correcting for the compaction measured to prestress the tuff samples to a hydrostatic stress state

Table 4. (Continued)

| DEPTH OF HOLE | TOTAL AIR-VOID CONTENT (%) | OFFSET AIR-VOID CONTENT (%) | INSITU AIR-VOID CONTENT (%) | INSITU BULK MODULUS (kbar) | MINIMUM BULK MODULUS (kbar) | PRESSURE RANGE OF MINIMUM (bars) |
|---|---|---|---|---|---|---|
| SUMMARY OF 1,2 AND 4 KBAR UNIAXIAL STRAIN TEST DATA | | | | | | |
| AVERAGE | 2.634 | 0.281 | 2.353 | 32.964 | | |
| STD.DEV. | 0.667 | 0.068 | 0.696 | 8.988 | | |
| STD.ERR. | 0.178 | 0.018 | 0.186 | 2.402 | | |
| SUMMARY OF ALL UNIAXIAL STRAIN TEST DATA | | | | | | |
| AVERAGE | | | | 31.812 | 11.109 | 211-310 |
| STD.DEV. | | | | 9.143 | 5.320 | 97-132 |
| STD.ERR. | | | | 2.286 | 1.330 | 24-33 |
| SUMMARY OF ALL DATA LESS MARKED HIGH AND LOW (H&L) POINTS | | | | | | |
| AVERAGE | | | 2.006 | 29.654 | 10.456 | |
| STD.DEV. | | | 0.510 | 3.508 | 3.276 | |
| STD.ERR. | | | 0.170 | 0.973 | 0.946 | |

Table 4. Summary of p-v compression data measured by Terra Tek in uniaxial strain tests on tuff samples from the U12G-OT-IH#1 and IH#2 drill holes.

| DEPTH OF HOLE | TOTAL AIR-VOID CONTENT (%) | OFFSET AIR-VOID CONTENT (%) | INSITU AIR-VOID CONTENT (%) | INSITU BULK MODULUS (kbar) | MINIMUM BULK MODULUS (kbar) | PRESSURE RANGE OF MINIMUM (bars) |
|---|---|---|---|---|---|---|
| | | | 4 KBAR UNIAXIAL TEST DATA | | | |
| 53.2 | 3.29 | 0.14 | 3.15 H | 27.5 | 5.00 L | 165-185 |
| 56.3 | 2.13 | 0.27 | 1.86 | 28.0 | 5.82 | 145-165 |
| 53.9 | 2.06 | 0.33 | 1.73 | 31.0 | 11.71 | 185-270 |
| 54.8 | 2.81 | 0.34 | 2.47 | 26.0 | 8.83 | 225-340 |
| 51.9 | 2.85 | 0.34 | 2.51 | 26.0 | 9.24 | 175-300 |
| 56.1 | 2.13 | 0.29 | 1.84 | 28.5 | 17.34 | 330-390 |
| AVERAGE | 2.545 | 0.285 | 2.260 | 27.833 | 9.657 | 239.58 |
| STD.DEV. | 0.509 | 0.077 | 0.551 | 1.862 | 4.484 | 74.59 |
| STD.ERR. | 0.208 | 0.031 | 0.225 | 0.760 | 1.830 | 30.45 |
| | | | 2 KBAR UNIAXIAL TEST DATA | | | |
| 23.5 | 4.01 | 0.21 | 3.80 H | 55.0 H | 14.05 | 495-700 |
| 52.8 | 2.65 | 0.26 | 2.39 | 33.0 | 10.63 | 225-300 |
| 55.0 | 1.68 | 0.41 | 1.27 | 38.5 | 21.77 H | 165-290 |
| 39.5 | 1.58 | 0.22 | 1.36 | 50.0 H | 21.27 H | 250-370 |
| 43.1 | 2.88 | 0.26 | 2.62 | 27.5 | 7.59 | 145-260 |
| AVERAGE | 2.560 | 0.272 | 2.288 | 40.800 | 15.462 | 320.00 |
| STD.DEV. | 0.993 | 0.080 | 1.037 | 11.503 | 6.451 | 160.29 |
| STD.ERR. | 0.444 | 0.036 | 0.464 | 5.144 | 2.885 | 71.69 |
| | | | 1 KBAR UNIAXIAL TEST DATA | | | |
| 14.0 | 2.78 | 0.27 | 2.51 | 30.0 | 4.24(l) | 125-165 |
| 56.3 | 2.74 | 0.26 | 2.48 | 33.0 | 12.85 | 225-350 |
| 54.8 | 3.29 | 0.34 | 2.95 | 27.5 | 10.70 | 270-370 |
| AVERAGE | 2.937 | 0.290 | 2.647 | 30.167 | 9.263 | 250.83 |
| STD.DEV. | 0.307 | 0.044 | 0.263 | 2.754 | 4.481 | 93.08 |
| STD.ERR. | 0.177 | 0.025 | 0.152 | 1.590 | 2.587 | 53.74 |
| | | | 0.5 KBAR UNIAXIAL TEST DATA | | | |
| 18.8 | 2.61 | ~0.45 | 2.16 | 18.5 L | 6.39 | 85-145 |
| 54.8 | 3.39 | ~0.33 | 3.06 | 29.0 | 10.32 | 165-360 |
| AVERAGE | 3.000 | | | 23.750 | 8.355 | 188.75 |
| STD.DEV. | 0.552 | | | 7.425 | 2.779 | 104.30 |
| STD.ERR. | 0.390 | | | 5.250 | 1.965 | 73.75 |

Table 3. Summary of unloading compressibility data for U12G-OT tuff derived from the slope of p-v curves obtained in uniaxial strain to 1, 2, and 4 kbar.

| HOLE DESIGNATION | DEPTH FT | PRESSURE 0 KB | 1 KB | 2 KB | 4 KB |
|---|---|---|---|---|---|
| U12G-OT-IH#1 | 53.2-55.0 | 105 | 120 | 132 | 220 |
| " | 56.3-57.8 | 70 | 80 | 125 | 225 |
| " | 53.9-54.5 | 83 | 87 | 125 | 225 |
| " | 54.8-56.3 | 85 | 87 | 110 | 175 |
| " | 51.9-58.2 | 88 | 104 | 120 | 175 |
| " IH#2 | 56.1-57.7 | 94 | 118 | 125 | 225 |
| SUMMARY | AVERAGE | 87.50 | 99.33 | 122.83 | 207.50 |
| OF 4 KBAR | STD. DEV. | 11.67 | 17.18 | 7.36 | 25.25 |
| DATA | STD. ERROR | 4.77 | 7.01 | 3.00 | 10.31 |
| U12G-OT-IH#1 | 23.5-24.5 | 107 | 131 | 160 | |
| " IH#2 | 52.8-53.2 | 78 | 130 | 185 | |
| " | 55.0-56.1 | 118 | 125 | 145 | |
| " IH#1 | 39.5-40.5 | 86 | 115 | 135 | |
| " | 43.1-44.1 | 75 | 125 | 130 | |
| SUMMARY | AVERAGE | 92.80 | 125.20 | 151.00 | |
| OF 2 KBAR | STD. DEV. | 18.83 | 6.34 | 22.19 | |
| DATA | STD. ERROR | 8.42 | 2.84 | 9.92 | |
| U12G-OT-IH#1 | 14.0-14.5 | | 133 | | |
| " | 56.3-57.8 | | 120 | | |
| " | 54.8-56.3 | | 120 | | |
| SUMMARY | AVERAGE | | 124.33 | | |
| OF 1 KBAR | STD. DEV. | | 7.51 | | |
| DATA | STD. ERROR | | 4.33 | | |
| SUMMARY | AVERAGE | 89.91 | 113.93 | 135.64 | 207.50 |
| OF ALL | STD. DEV. | 14.75 | 17.51 | 20.99 | 25.25 |
| DATA | STD. ERROR | 4.45 | 4.68 | 6.33 | 10.31 |

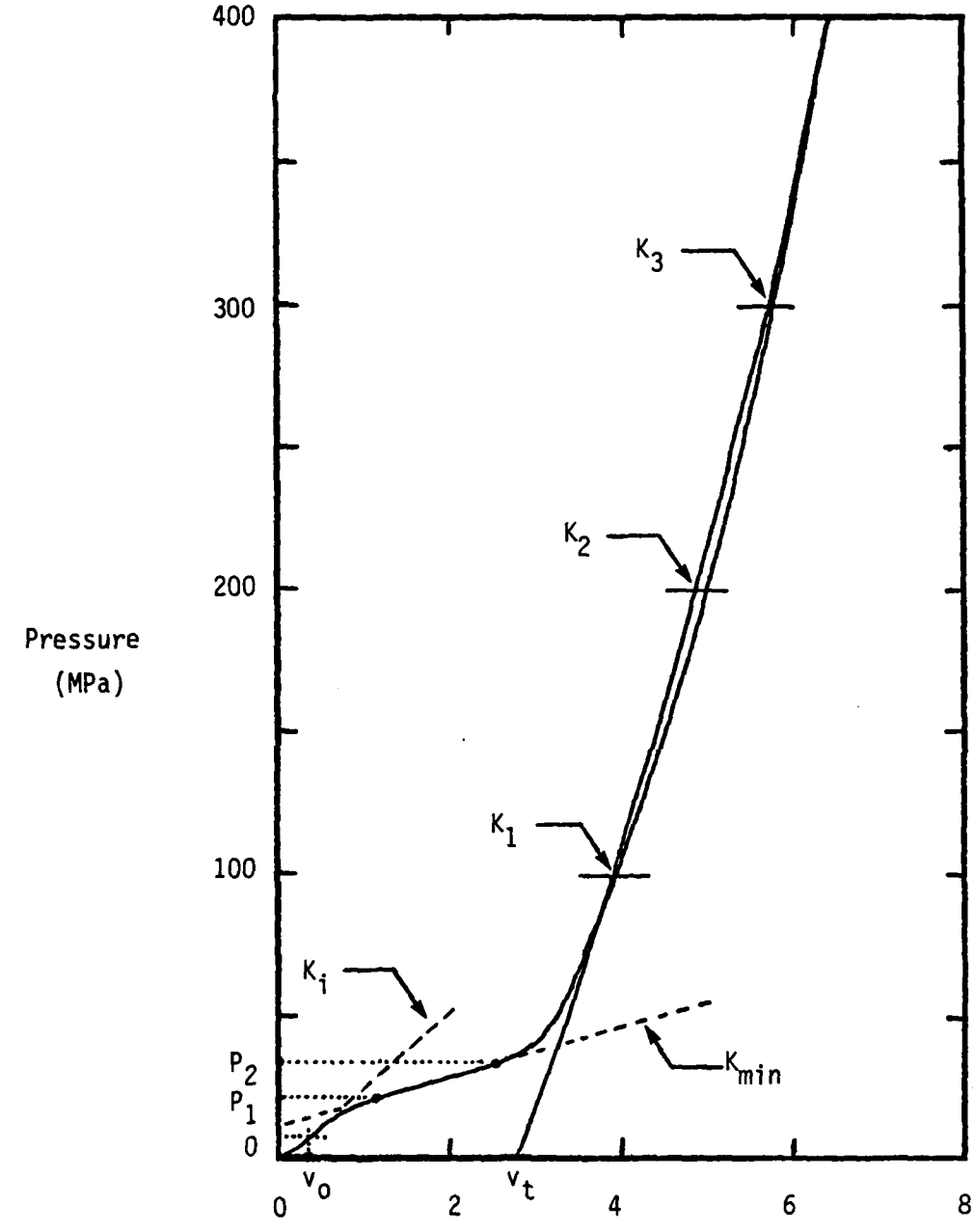


Figure 1. Typical p-v response measured by Terra Tek on U12G-OT core showing fit parameters summarized in Tables 3 and 4.

Table 2. Calculated physical properties and ultrasonic moduli for tuff samples taken in U12N.12, U12N.15, U12N.18 and U12G-OT.

| PHYSICAL PROPERTY | U12N.12 PRESHOT | U12N.12 | U12N.15 | U12N.18 | U12G-OT |
|---|---|---|---|---|---|
| | | VALUES FROM TABLE 1 | | | |
| AMBIENT DENSITY | 1.9217 | 1.8627 | 1.88-1.87 | 1.8347 | 2.0140 |
| DRY DENSITY | 1.5894 | 1.4947 | 1.52-1.49 | 1.4740 | 1.7100 |
| GRAIN DENSITY | 2.4315 | 2.4467 | 2.46-2.48 | 2.4247 | 2.5080 |
| Cp (km/s) | 3.1054 | 3.1343 | 2.45-2.93 | 2.7693 | 3.2520 |
| Cs (km/s) | 1.5120 | 1.3367 | 1.96-1.20 | 1.2507 | 1.7160 |
| | | CALCULATED VALUES | | | |
| AIR VOLUME | 0.01403 | 0.02110 | 0.0221-0.0192 | 0.03139 | 0.01418 |
| LIQUID VOLUME | 0.33230 | 0.36800 | 0.3600-0.3800 | 0.36070 | 0.30400 |
| SOLID VOLUME | 0.65367 | 0.61090 | 0.6179-0.6008 | 0.60791 | 0.68182 |
| POROSITY | 0.34633 | 0.38910 | 0.3821-0.3992 | 0.39209 | 0.31818 |
| SATURATION | 0.95949 | 0.94578 | 0.9421-0.9519 | 0.91994 | 0.95543 |
| WET WEIGHT | 0.17292 | 0.19756 | 0.1915-0.2032 | 0.19660 | 0.15094 |
| POISSON'S RATIO | 0.3446 | 0.3888 | 0.4093-0.3992 | 0.37188 | 0.3071 |
| YOUNG'S MODULUS (KBAR) | 118.15 | 92.45 | 48.84-75.36 | 78.74 | 155.0 |
| BULK MODULUS (KBAR) | 126.74 | 138.61 | 89.75-124.63 | 102.44 | 133.9 |
| RIGIDITY MODULUS (KBAR) | 43.93 | 33.28 | 17.33-26.93 | 28.70 | 59.3 |

A number of related properties and elastic moduli can be derived from the information in Table 1. For completeness, these derived properties are listed in Table 2. Note that all moduli in Table 2 are ultrasonic unless otherwise noted.

## 2.3 POROUS CRUSH RESPONSE

In general, NTS tuffs show a considerable variation in the details of their p-v response, even for adjacent samples taken from apparently uniform beds. The U12G-OT tuff is no exception. In previous studies the general approach has been to overlay the entire p-v data base developed from uniaxial load-unload tests in the form of crush curves. The curve judged to be most representative of the set as a whole, adjusted slightly for the air-void content, if required, is then selected. Since the numerical model of the crush response of the tuff is specified using a relatively sophisticated spline-fitting routine, the p-v response data can be represented very accurately. In the present case a more quantitative approach to the definition of an average crush response was desirable, even though it was not at all clear that an appreciable difference in the tuff behavior was likely to result.

Of course, in order to develop the "best" fit to the data it was necessary to decide which features of the data were of primary importance. An additional complication arose from the graphical form of the p-v uniaxial test data since "numbers" were needed for each feature of the data for which an average was desired. The features of the Terra Tek p-v data chosen for analysis were the initial slope of the crush curve, the minimun slope on the "toe" of the crush curve, the limits of this soft regime, the pressure of approximately complete compaction (i.e., the crush pressure), and the bulk modulus of the fully compacted material at selected pressures on unload. These features are illustrated schematically in Figure 1, and the values derived from rather tedious graphical measurements of the data are summarized in Tables 3 and 4. To avoid combining dissimilar data sets, data in these tables are segregated by the value of maximum confining pressure achieved in the test. Additionally, values which appear to be outside the expected scatter limits are indicated as "high" (H) or "low" (L) in Tables 3 and 4.

Earlier p-v measurements in tuff often showed an extremely soft modulus at the

Table 1. Average physical properties from tuff core samples taken in drill holes U12N.12, U12N.15, U12N.18 and U12G-OT.

| PROPERTY | U12N.12 PRESHOT | U12N.12 | U12N.15 | U12N.18 | U12G-OT |
|---|---|---|---|---|---|
| AMBIENT | 1.9217 | 1.8627 | 1.88-1.87 | 1.8347 | 2.0140 |
| DENSITY | 0.0726 | 0.0935 | | 0.0657 | 0.0581 |
| ($gm/cm^3$) | 0.0101 | 0.0242 | | 0.0170 | 0.0260 |
| DRY | 1.5894 | 1.4947 | 1.52-1.49 | 1.4740 | 1.7100 |
| DENSITY | 0.1263 | 0.1435 | | 0.0961 | 0.0765 |
| ($gm/cm^3$) | 0.0175 | 0.0371 | | 0.0248 | 0.0342 |
| GRAIN | 2.4315 | 2.4467 | 2.46-2.48 | 2.4247 | 2.5080 |
| DENSITY | 0.0399 | 0.0504 | | 0.0331 | 0.0545 |
| ($gm/cm^3$) | 0.0055 | 0.0130 | | 0.0086 | 0.0244 |
| Mw | 18.0269 | 19.9133 | 19.2-20.1 | 19.7400 | 15.1200 |
| (%) | 2.7912 | 3.6584 | | 2.5489 | 1.3517 |
| | 0.3871 | 0.9446 | | 0.6581 | 0.6045 |
| POROSITY | 34.6058 | 38.8933 | 38.2-39.9 | 39.1800 | 31.8200 |
| (%) | 5.6646 | 5.8702 | | 4.1845 | 2.1568 |
| | 0.7855 | 1.5157 | | 1.0804 | 0.9646 |
| SATURATION | 95.9423 | 94.8000 | 94.4-95.3 | 92.1533 | 95.6400 |
| (%) | 2.3545 | 2.8854 | | 4.2069 | 1.6637 |
| | 0.3265 | 0.7450 | | 1.0862 | 0.7440 |
| CALC VOIDS | 1.3692 | 2.0933 | 2.2-1.9 | 3.1140 | 1.4000 |
| (%) | 0.7353 | 1.3541 | | 1.7191 | 0.5339 |
| | 0.1020 | 0.3496 | | 0.4439 | 0.2387 |
| MEASURED | 2.0419 | 1.7143 | | 2.4533 | |
| COMPACTION | 1.4163 | 0.8995 | | 0.9164 | |
| (%) | 0.2160 | 0.2404 | | 0.2366 | |
| Cp | 3.1054 | 3.1343 | 2.45-2.93 | 2.7693 | 3.2520 |
| Ultrasonic | 0.4100 | 0.3835 | | 0.2540 | 0.3196 |
| (km/s) | 0.0569 | 0.0990 | | 0.0656 | 0.1429 |
| Cs | 1.5120 | 1.3367 | 0.96-1.20 | 1.2507 | 1.7160 |
| Ultrasonic | 0.2925 | 0.1938 | | 0.2272 | 0.2314 |
| (km/s) | 0.0414 | 0.0104 | | 0.0607 | 0.1035 |
| POISSON'S | 0.3446 | 0.3875 | 0.41-0.40 | 0.3716 | 0.3056 |
| RATIO | 0.0330 | 0.0215 | | 0.0382 | 0.0339 |
| | 0.0047 | 0.0055 | | 0.0102 | 0.0152 |

NOTE: U12N.12 preshot - 52 samples, U12N.12 - 15 samples, U12N.15 - unknown, U12N.18 - 15 samples and U12G-OT - 5 samples. Numbers listed are average value, standard deviation and standard error of the mean.

domain is specified by the shear modulus through its dependence on the degree of air-void crush and the deviatoric stress state. In the plastic regime, tuff strength, as specified by a yield surface, controls the maximum allowable stress difference. The yield surface for ONE-TON tuff is modeled in this study as a function of both strain rate and degree of damage incurred by the tuff during its earlier deformation.

The static Terra Tek material response tests[2] and the dynamic SRI shot data[3] suggest that the ONE-TON tuff exhibits behavior not usually modeled in ground motion calculations. In particular, dilatant response was widely observed in the Terra Tek data, while the wave speeds observed in the explosive SRI test are clearly inconsistent with the static moduli. The latter phenomenon is accounted for in the computations through the use of a viscoelastic model in the form of a standard linear solid.

## 2.2 PHYSICAL PROPERTIES

Physical properties from five G-Tunnel, U12G-OT samples were reported by Terra Tek.[2] In the same time frame, Terra Tek determined physical properties for a much larger number of N-Tunnel tuff samples. Given the relatively limited number of G-Tunnel samples, it was felt that it could be enlightening to compare the G-Tunnel data with that for N-Tunnel. Such a comparison is made in Table 1, where average, standard deviation and standard error of the mean values are given in that order for each physical property. Several conclusions can be drawn from Table 1. Within the uncertainty of the data, scatter (i.e., standard deviation) in the G-Tunnel properties is quite comparable to the N-Tunnel experience. Secondly, there appears to be a statistically significant difference between G-Tunnel and N-Tunnel tuffs. The G-Tunnel tuff porosity is appreciably less ($\sim 32\%$ vs. $\sim 39\%$), while the saturation (95%) is comparable, leading to a relatively high ambient density and low water content in G-tunnel tuff. Additionally, the G-Tunnel tuff appears to have somewhat elevated ultrasonic wave speeds, particularily for the ultrasonic shear wave velocity. A final point to be made from Table 1 is the calculated air-void value of $\sim 1.4 \pm 0.24\%$ will be seen to be at variance with the air-void content ($\sim 2.5\%$) inferred from uniaxial compaction tests to 400 MPa.

employed for a number of years at PacTech. For example, good agreement with the observed uniaxial and triaxial loading response for 2C4 grout was achieved by allowing the shear modulus to soften during loading[10]. A reversible formulation of this shear modulus model, however, implies an increasing shear modulus on unload; behavior at odds with the observed response of all tuffs with which we are familiar. Figure 4 shows all of the ONE-TON effective unloading shear modulus data plotted as a function of stress difference. The trend of the data is evident and seen to be independent of the maximum confining stress experienced by the tuff. In contrast, poor correlation is observed when these data are plotted as a function of pressure or confining stress. Uniaxial test reloading data were not obtained for the ONE-TON tuff; however, cycled uniaxial test data are available for N-Tunnel tuff,[11] an example of which is shown in Figure 5. A plot of 54 data points derived from the U12n.18 data set[4] shows reasonable accord with the G-Tunnel tuff behavior illustrated in Figure 4 giving us some confidence that cycled N-Tunnel tuff data can be used to guide the behavior of the variable shear modulus model used in these studies.

A shear modulus model was constructed to incorporate the unloading behavior illustrated in Figure 4, as well as the hysteretic reloading response shown in the cycled N-Tunnel data (Figure 5). In this model the shear modulus was made a function of the deviatoric stress summarized by Equations 1 and 2. During loading the shear modulus is given by

$$G = GMIN - DELG \left( \frac{SJ2P}{SJ2PM} - 1.0 \right) \tag{1}$$

and during unload

$$G = GMIN + DELG \left( \frac{SJ2P}{SJ2PM} \right) \tag{2}$$

where SJ2P is the second invarient of the stress tensor and the other parameters are constants given in Table 6 for the G-Tunnel tuff model used in this study. During

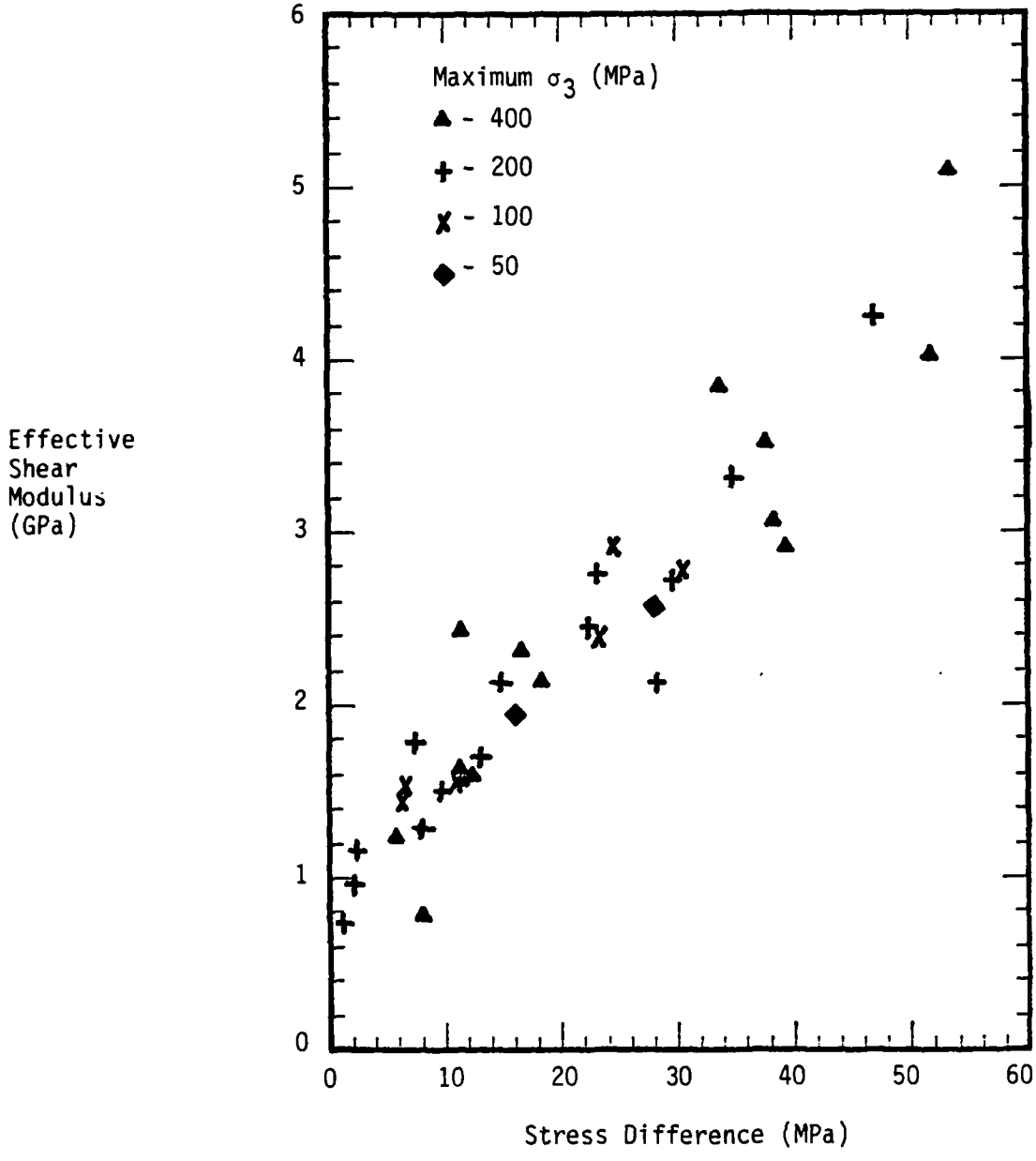


Figure 4. Effective shear modulus measured from uniaxial unloading response of U12G-OT tuff.

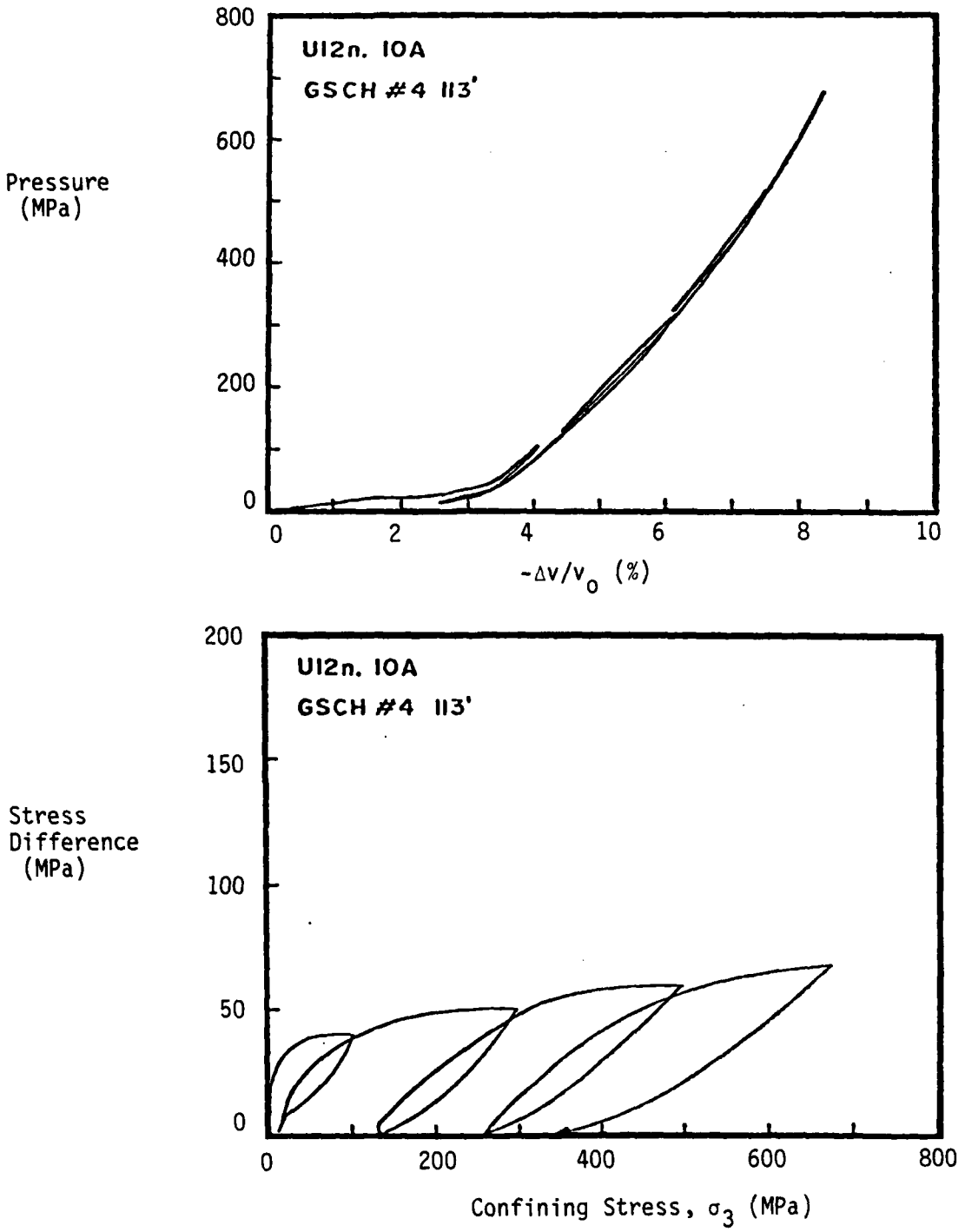


Figure 5. Cycled uniaxial test data obtained by Terra Tek[11] showing hysteresis in the unloading-reloading response.

unloading the shear modulus was not allowed to fall below a minimum value given by GML.

Table 6. Effective shear modulus parameters used to model the response of G-Tunnel tuff.

| PARAMETER | VALUE (MPA) |
|---|---|
| GMIN | 1000 |
| SJ2PM | 30 |
| DELG | 2000 |
| GML | 1500 |

The behavior of the numerical model in response to a hypothetical cycled uniaxial test sequence is shown in Figure 6. The correspondence to the N-Tunnel data given in Figure 5, while not exact, would seem to be quite adequate given the desire to couch the model in relatively simple terms and in view of the evident improvement over earlier shear modulus models. Another demonstration that the model captures the right qualitative behavior of the material is shown in Figure 7. Unfortunately, the virgin strength of this particular sample was unusually high. Allowing for this limitation, the model gives rather remarkable agreement with data taken on a stress-strain path significantly different from that which was used to develop the variable shear modulus formulation.

Given a reasonable value for the shear modulus, the computed stress and velocity histories for the SRI and ONE-TON tests will be relatively independent of the details of the shear modulus model. This is a result of the dominant influence of the void crush and plastic response models on the dynamic stresses and motion induced in the tuff during the time of interest in the explosive test data. It should be noted, however, that the elastic response model strongly influences the residual stress state ultimately calculated in the medium around the cavity. Thus, the proper shear modulus formulation is an important

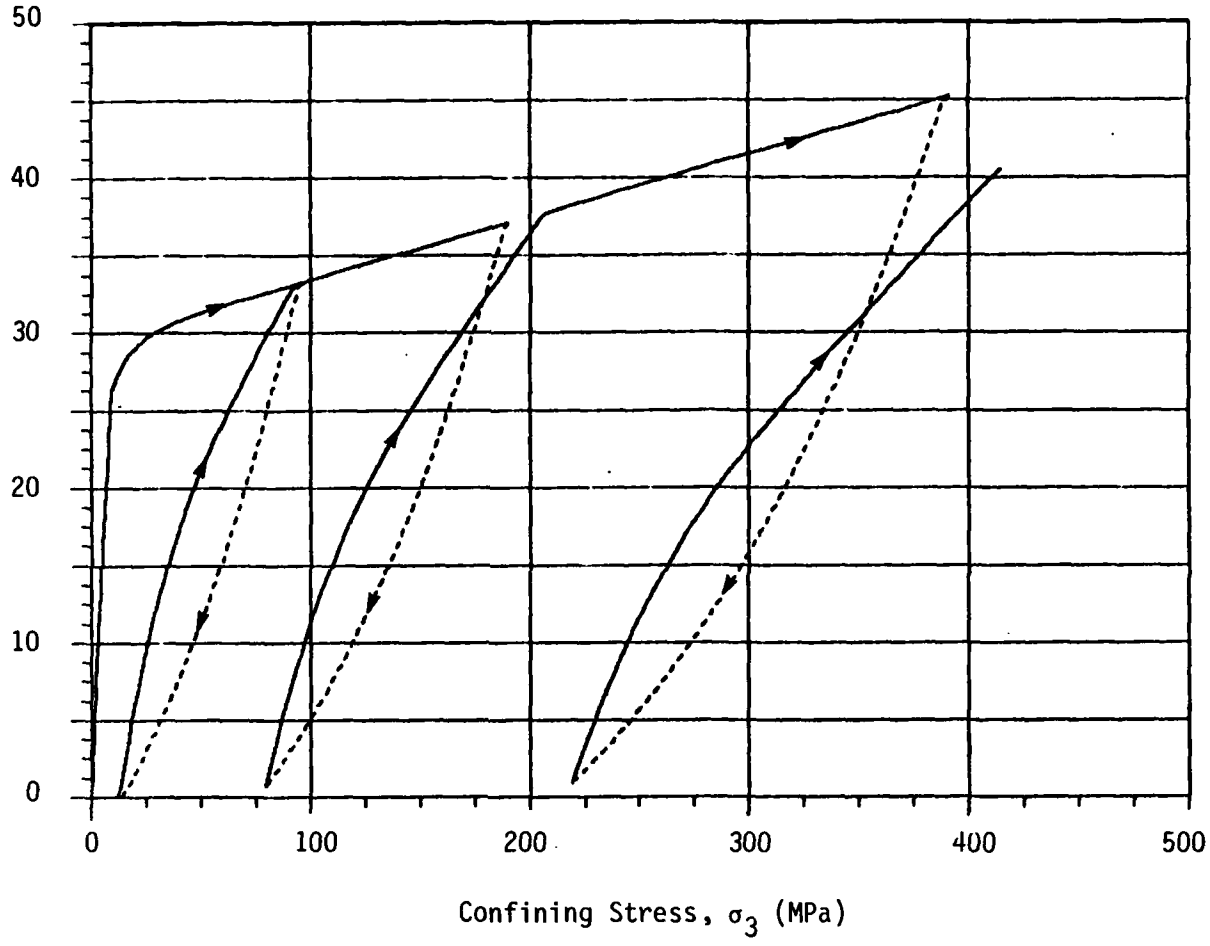


Figure 6. Numerical model uniaxial test, cycled response.

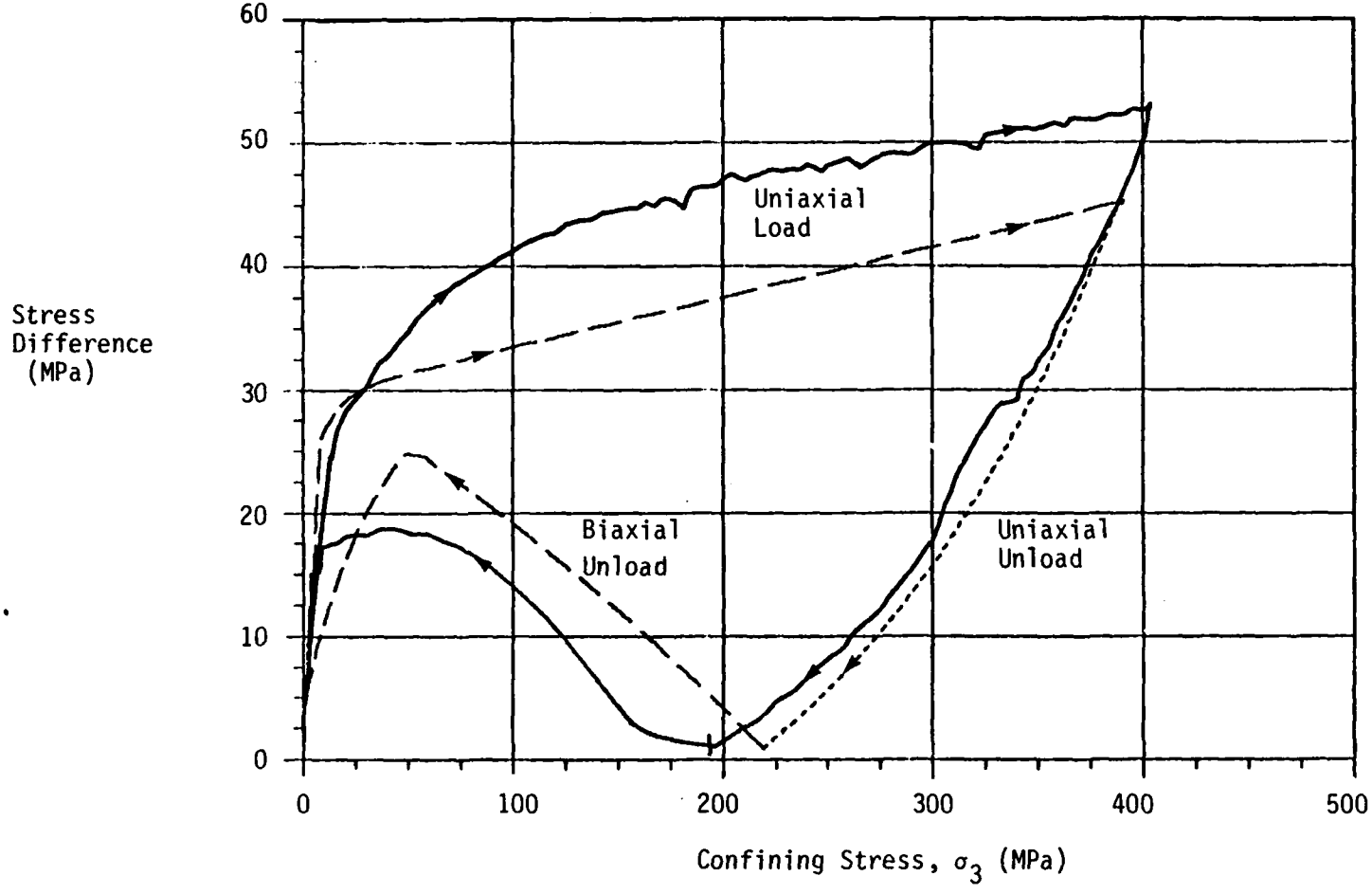


Figure 7. Comparison of calculated G-Tunnel tuff response (dashed and broken line) with Terra Tek data (solid line) for a uniaxial load, uniaxial unload, biaxial unload test sequence.

containment issue that has been addressed numerically in this study, but which cannot be tested by the existing data set from these experiments.

## 2.5 VIRGIN AND DAMAGED YIELD STRENGTH MODELS

The notions of failure and yield are relatively subtle in earthen materials in comparison with textbook examples for simple materials. In particular, the granular nature of these media presents numerous possible mechanisms (e.g., dilation, porous flow and pore pressure effects, shear banding, evolution of the grain size and shape, etc.) whereby the strength of the medium may be expected to be a complex function of the stress-strain path as well as the stress-strain rate. It is well known that the strength of tuff as measured by peak stress difference in triaxial tests on undamaged samples is appreciably higher (on the order of 20%) than the apparent strength as seen in a uniaxial test at the same confining stress. From a materials point of view, such behavior could be couched in terms of a strain hardening model. On the other hand, evidence from a variety of different recent research efforts strongly suggests that tuff which has undergone large-strain deformations suffers a gross reduction in strength, at least at lower levels of confining stress (say, below 50 MPa). Finally, as will be discussed in the following sections, very substantial strain rate effects on the tuff strength are implied by the failure of the SRI small scale explosive tests to scale to the results of the ONE-TON shot.

One of the primary goals of the quasi-static material property testing program was to provide a more satisfactory definition of the deviatoric response of the tuff along the most relevant stress-strain (but not strain rate) path. Earlier material test programs at Terra Tek investigated some aspects of strength degradation for large strain triaxial stress tests (little effect noted) and studied the tuff response to a series of load-unload uniaxial strain paths (strong effects in some aspects of the response were evident)[11,12].

An examination of calculated stress-strain paths in tamped spherical explosions suggests that the motion can crudely be considered to undergo three characteristic types of deformation. Initially, an element of material is compressed in a state of nearly pure uniaxial strain as the shock front passes through it. This portion of the load covers the entire loading process up to the peak stress state; however, it only accounts for a very

brief portion of the total deformation history. Following the uniaxial loading phase, the shocked material tends to unload along a biaxial strain path, i.e., along a path of fixed radial strain and dilational transverse strain. This portion of the deformation history varies considerably in importance with range from the charge, being much more important at the more distant stations, and generally is not along as 'pure' a biaxilal strain path as seen in the uniaxial loading phase. Finally, the material completes its deformation following a relatively complex stress-strain path at moderate to low levels of stress during which it coasts outward, rebounds, and then oscillates elastically at an ever decreasing amplitude.

Clearly, material response data taken in uniaxial strain does not approximate the strain path followed by the material in the spherical explosive tests in tuff. On the other hand, it is neither reasonable nor possible to attempt to trace out the details of the tuff motion in stress-strain space in the laboratory, and the incorporation of such generalized strain path data in the models in other than an ad hoc fashion would be an impossible task. The approach adopted in this program was to considerably broaden the scope of the materials testing program to include several different types of biaxial unloading test sequences followed by either a triaxial test at a reduced confining pressure or by a series of cycled uniaxial load, biaxial unload strain paths. The objective was to much more completely define the onset, progression and magnitude of the material damage process in tuff.

Because some of the cycled material test data were not available until after much of the numerical calculations had been completed, the damaged yield strength model developed in this study relied more heavily on data taken earlier in this program[2]. Early test data had the interesting feature of initially increasing the stress difference on biaxial unload. Subsequent biaxial unloading data did not reproduce this behavior, with the biaxial unloading falling on or below the uniaxial loading response as illustrated in Figure 8. Thus there remains some unresolved uncertainty in this aspect of the tuff unloading response. But magnitude of this effect is quite modest so that its inclusion or omission in the damaged strength model was found to have little influence in the calculated waveforms.

As might be expected, the strength of the damaged tuff as defined by the triaxial

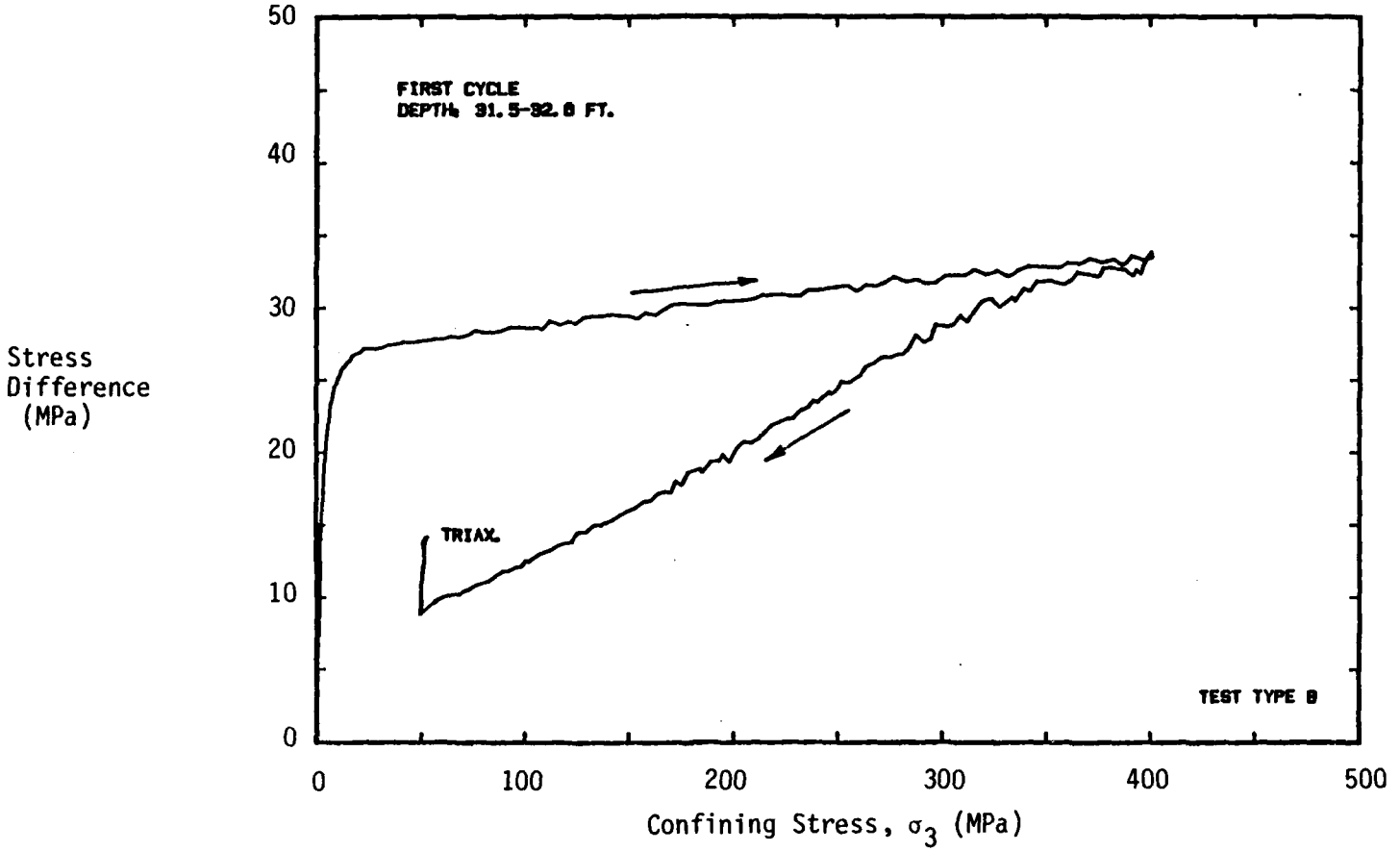


Figure 8. Typical uniaxial load, biaxial unload, traixial reloading response measured by Terra Tek[2] for U12G-OT tuff.

test data was significantly higher than the apparent strength as inferred from the biaxial unloading response. That is, as is observed in the response of virgin tuff, damaged tuff also appears to strain harden (see Figure 8). Rather than attempt to explicitly model the hardening behavior of the tuff, we assumed that the damaged failure surface defined by the triaxial test results would be more characteristic of the tuff strength during most of the dynamic coasting phase of the tuff motion. Use of a lower damage strength curve based on the biaxial unloading path data lengthens the negative phase of the calculated motion, but again the effect is relatively modest.

All calculations except those explicitly modeling dilatation used a non-associative flow rule with radial return to the yield surface. The more general non-associative rule formulation used in the dilatational study is described in Section 2.7. The static yield surface used to describe the virgin tuff response in the baseline computations is given by

$$Y_u = 29 + 0.04p - 18 \exp\{-0.092p\} \quad (3)$$

where $Y_u$ and the pressure, p, are expressed in units of MPa. Similarily, the damaged response was modeled as

$$Y_d = 24 + 0.08p - 21 \exp\{-0.030p\} \, . \quad (4)$$

Material was considered to lie on the undamaged failure surface (Equation 3) so long as the specific volume continued to decrease, i.e., during the loading phase of the deformation.

As discussed in Section 3, it was necessary to modify the static failure surfaces defined in Equations 3 and 4 to account for strain rate hardening in the SRI test data. A simple logarithmic formulation for the dynamic yield strength, Y', was was adopted in this study

$$Y' = Y[1.67 + 0.33 \log |\dot{\varepsilon}_r|] \quad (5)$$

where Y is the static yield strength given by either Equation 4 or 5, $\dot{\varepsilon}$ is the radial strain rate and a static rate of $10^{-2}$ is assumed (i.e., Y' > Y). In addition, both the virgin and damaged yield surfaces were modified by the usual energy dependent thermal softening formulation $(1-e/e_m)$, where the melt energy $e_m$ was taken to be $1.91 \times 10^{10}$. The yield strength reduction introduced by this correction is small at the relatively low internal energies encountered in the HE driven tuff in this study.

## 2.6 VISCOELASTIC MODEL

One model that was found to be useful in matching the velocity traces produced by SRI was a viscoelastic model, generally referred to as the standard linear solid. This viscoelastic model is formulated in terms of a relaxation law given by

$$p(t) = \int_0^t M(t-t')\dot{\varepsilon}(t')\, dt' \quad , \quad (6)$$

where p is the pressure, $\dot{\varepsilon}$ is the volumetric strain rate and M is called the relaxation function. For the standard linear solid M is given by

$$M(t) = M_\infty + \Delta M \exp(-\beta t) \quad , \quad (7)$$

where $M_\infty$ is the late time modulus, $M_\infty + \Delta M$ is the early time modulus, and $1/\beta$ is the relaxation time that sets the scale between the two time regimes.

Some further insight into this formulation can be gotten by Fourier transforming the relaxation equation

$$p(\omega) = i\omega M(\omega) \varepsilon(\omega) \quad , \tag{8}$$

with $i\omega M(\omega)$ given by

$$i\omega M(\omega) = M_\infty + \frac{i\omega}{i\omega + \beta} \Delta M \quad . \tag{9}$$

Equation 3 has a simple form reminiscent of the linear elastic constitutive relations except now the modulus is frequency dependent. At frequencies high with respect to $\beta$ the modulus is given by

$$i\omega M(\omega) \simeq M_\infty + \Delta M \quad ; \qquad \omega >> \beta \quad , \tag{10}$$

and a low frequencies the modulus becomes

$$i\omega M(\omega) \simeq M_\infty \quad ; \qquad \omega << \beta \quad . \tag{11}$$

There are two moduli or wave speeds associated with this material model. High frequency components of a pulse travel with the wave speed corresponding to the high frequency modulus and the low fequency components of the pulse travel with the the low frequency wave speed, with $\beta$ setting the scale of the crossover region. By adjusting these two wavespeeds it is possible to disperse the pulse and thereby increase the rise time of the wave.

This model was used to define the volumetric response of G-Tunnel tuff. The low frequency response was given by a Tillotsen equation of state with a zero pressure modulus of 80 kbar and a bulk modulus of 120 kbar at a pressure of 4 kbar. A modulus

increment, $\Delta M$, of 200 kbar and relaxation time, $1/\beta$, of 0.2 $\mu s$ were found to best fit the SRI velocity traces.

## 2.7 DILATATION RESPONSE

Some of the static tests described above show that G-tunnel tuff undergoes dilatant response when subjected to both a triaxial load or biaxial unload after a uniaxial load. A model was postulated to account for this behavior and was used in a simulation of the ONE-TON event.

Since no dilatation is seen in tests consisting of a uniaxial load followed by a uniaxial unload a dilatation model based on a plastic flow rule was chosen. The idea is to introduce the air-voids during plastic flow. This is accomplished by using a general form of a non-associated flow rule.

During each time step of the calculation the deviatoric stress is updated using the shear modulus and the computed strain increment. In general, it is possible for the computed deviatoric stress state to lie outside the yield surface. When this occurs, a prescription, or flow rule, is required to specify how to reduce the deviatoric stresses to a point lying on the yield surface.

To formulate this flow rule, it is useful to consider the plot of yield strength against pressure shown in Figure 9. The point 'A' shown in Figure 9 represents a hypothetical value for the deviatoric stress obtained in the stress update section of a calculation. The goal is to find the point 'B' on the yield surface that properly describes the final state of stress achieved by material at the end of the time step.

Various procedures have been suggested. Generally, they involve specifying an angle with respect to the tangent of the yield surface, and require finding a line that passes through the point of interest and intersects the yield surface at the specified angle. The point of intersection on the yield surface is the final state of stress achieved by the material. An example of such a construction is shown in Figure 9.

Depending on the angle chosen, the pressure of the material can be altered by the

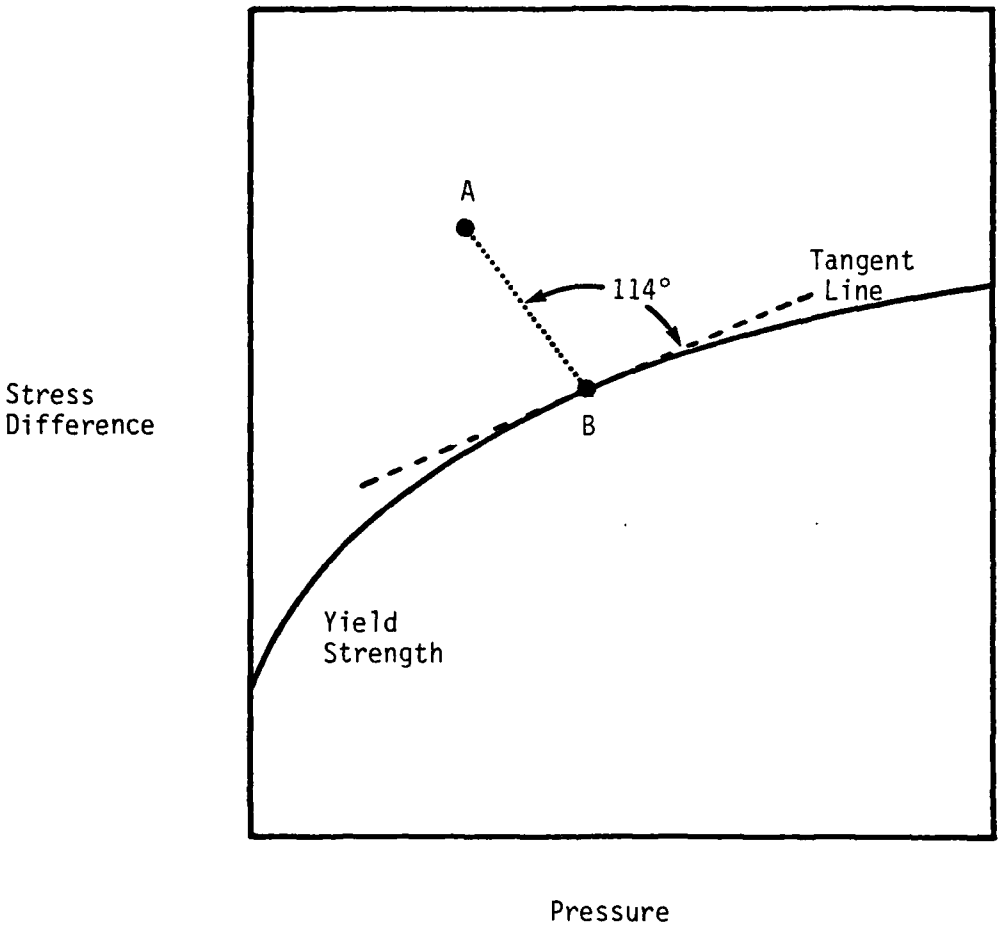


Figure 9. Sketch of hypothetical yield surface illustrating generalized associated flow rule adopted in dilatation calculations.

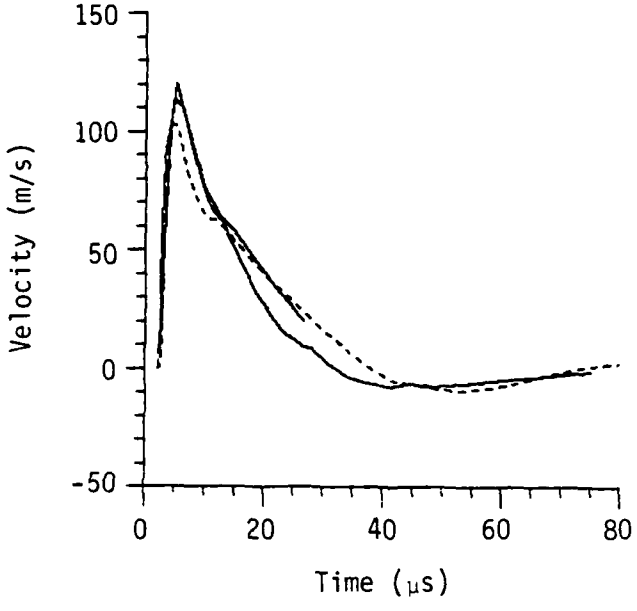


(a) r=1.27 cm

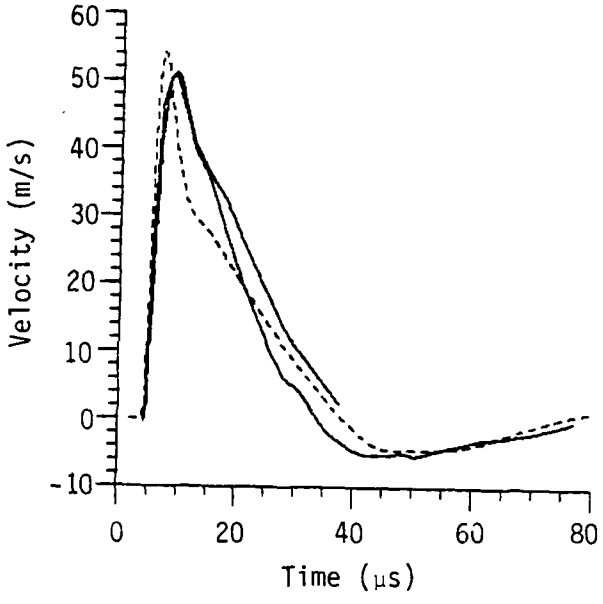


(b) r=1.90 cm

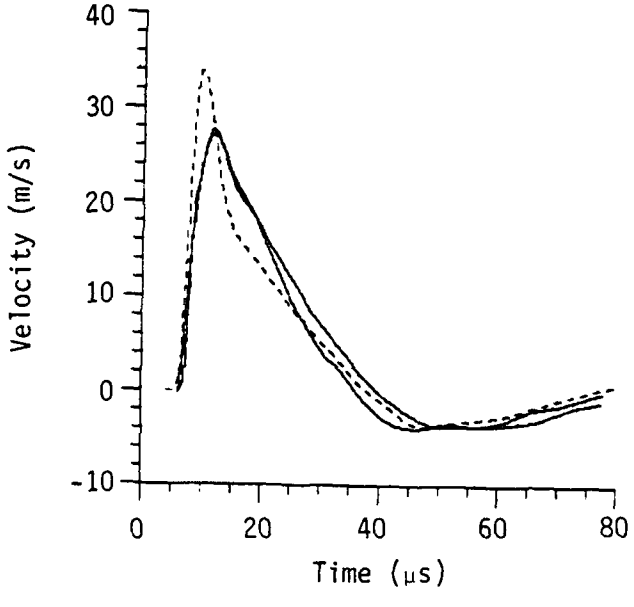


(c) r=2.54 cm

Figure 18. Comparison of SRI experiment data (solid) with a calculation (dashed) using a viscoelastic model and no air-void content.

was chosen to round the peak and lengthen the rise-time of the pulse. This model postulates two bulk moduli, one used for rapid loading and one for slow loadings. In effect, the first arrival is governed by the high frequency modulus and the peak arrival by the low frequency one. This can be accomplished with a suitable choice for the relaxation time which sets the scale for the crossover between the two frequency domains. By varying these two moduli it is possible to change the time between the first and peak arrival thereby rounding the pulse and increasing the rise time.

A comparison of the results of a calculation using the viscoelastic model and experiment is shown in Figures 18 and 19. The rise time and peak behavior is quite close and the attenuation rate is also in much better agreement. Overall, considerable improvement was obtained using this model. The price has been to use a model that does not agree with the the static test results obtained by Terra Tek.

A complication seen in the material response is the evidence of dilatancy both in the lab data and the SRI experiments. The static test results were discussed in Section 2. The dilatancy measured by the SRI experiments is shown in Figure 20.[15] The curves show the degree of volumetric strain produced between succesive stations. There is a net expansive volumetric strain seen in the material between the 1.27 and 1.90 cm stations, however, there is very little net compaction or expansion seen between the further downrange stations. This explains, in part, why the models with very little or no air-void content did so well.

In summary, the predictions based on the Terra Tek data did not do very well. Two major issues were raised by this lack of agreement. The first concerned the attenuation rate of peak velocity and its implications concerning the true air-void content of the tuff needed for consistency with this attenuation rate. Perhaps the inconsistency between statically measured air-void content and the observed attenuation rate can be accommodated with an appropriate dilatancy model, and work is being done in this vein. Alternatively, as discussed in Section 2, the tuff may well actually have a much lower air-void content in situ than that implied by laboratory measurements. The second problem raised by the SRI data is the long rise time and rounded peak observed in the velocity traces. A material response model was proposed that matched the measured wave shapes quite well, but it abandoned both the porous crushup behavior and the

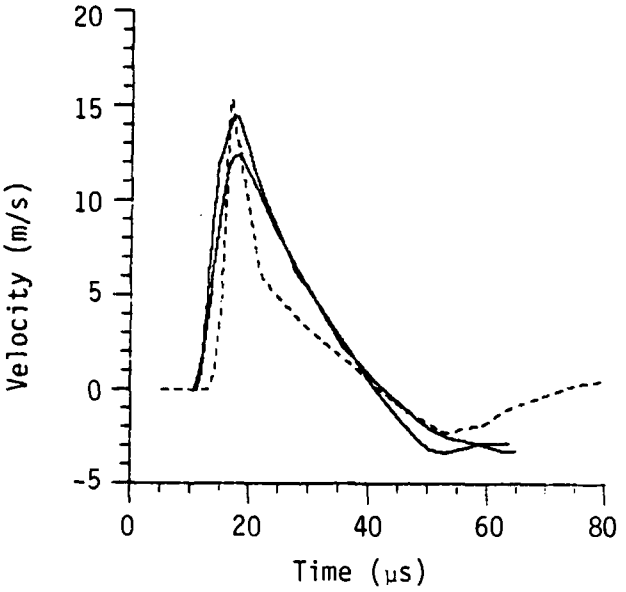


(a) r=4.0 cm

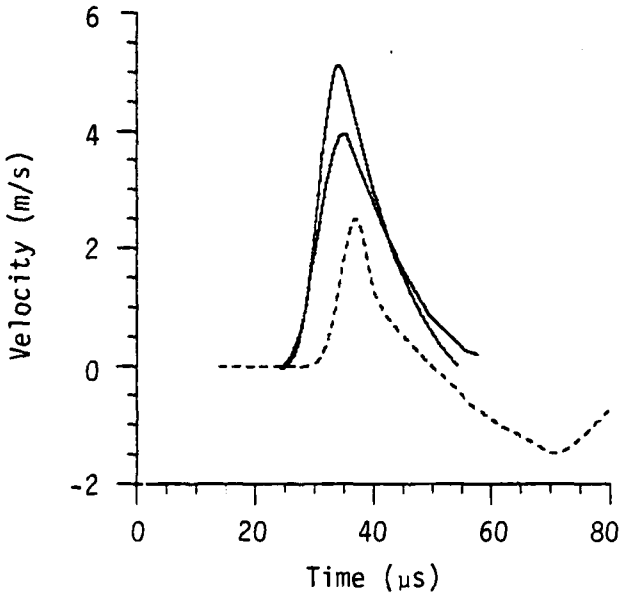


(b) r=8.0 cm

Figure 17. Comparison of SRI experiment data (solid) with a calculation (dashed) using 0.69%.

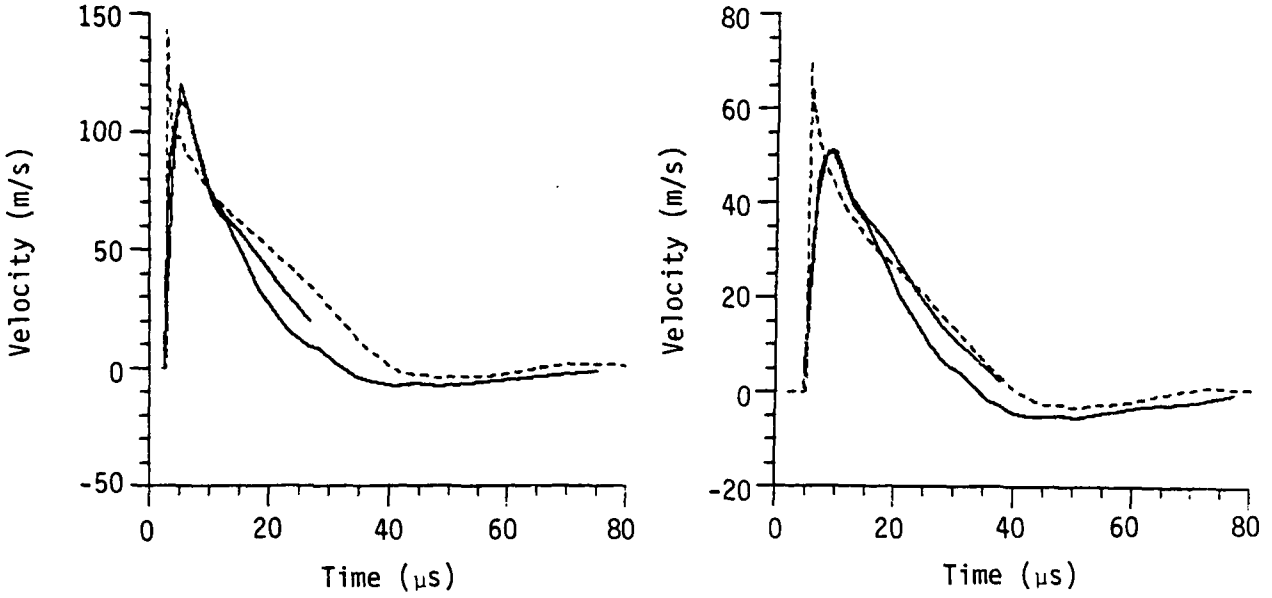


(a) r=1.27 cm




(b) r=1.90 cm

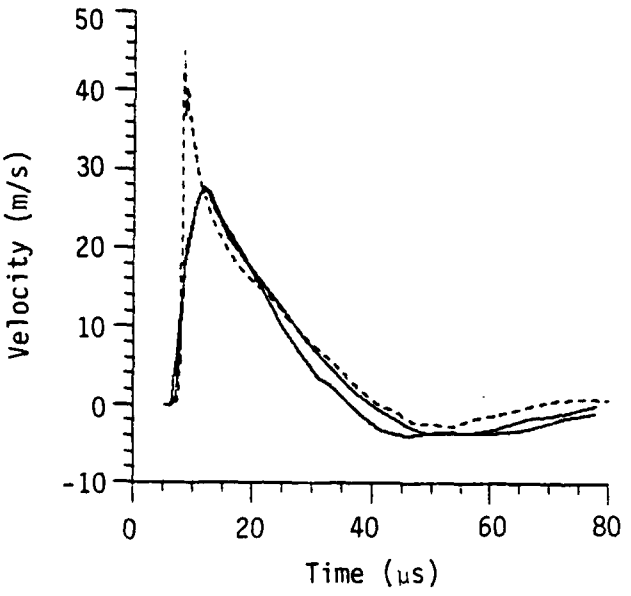


(c) r=2.54 cm

Figure 16. Comparison of SRI experiment data (solid) with a calculation (dashed) using 0.69% air-void content.

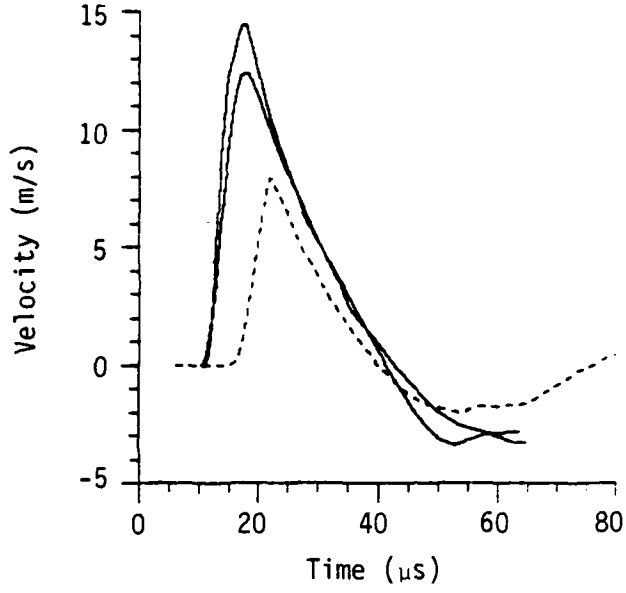


(a) r=4.0 cm

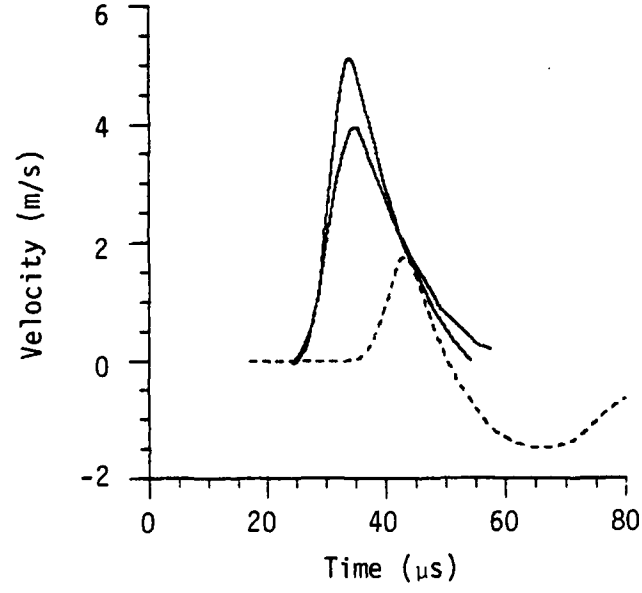


(b) r=8.0 cm

Figure 15. Comparison of SRI experiment data (solid) with calculation (dashed) using 2.2% air-void content and strain rate hardening on all the time.

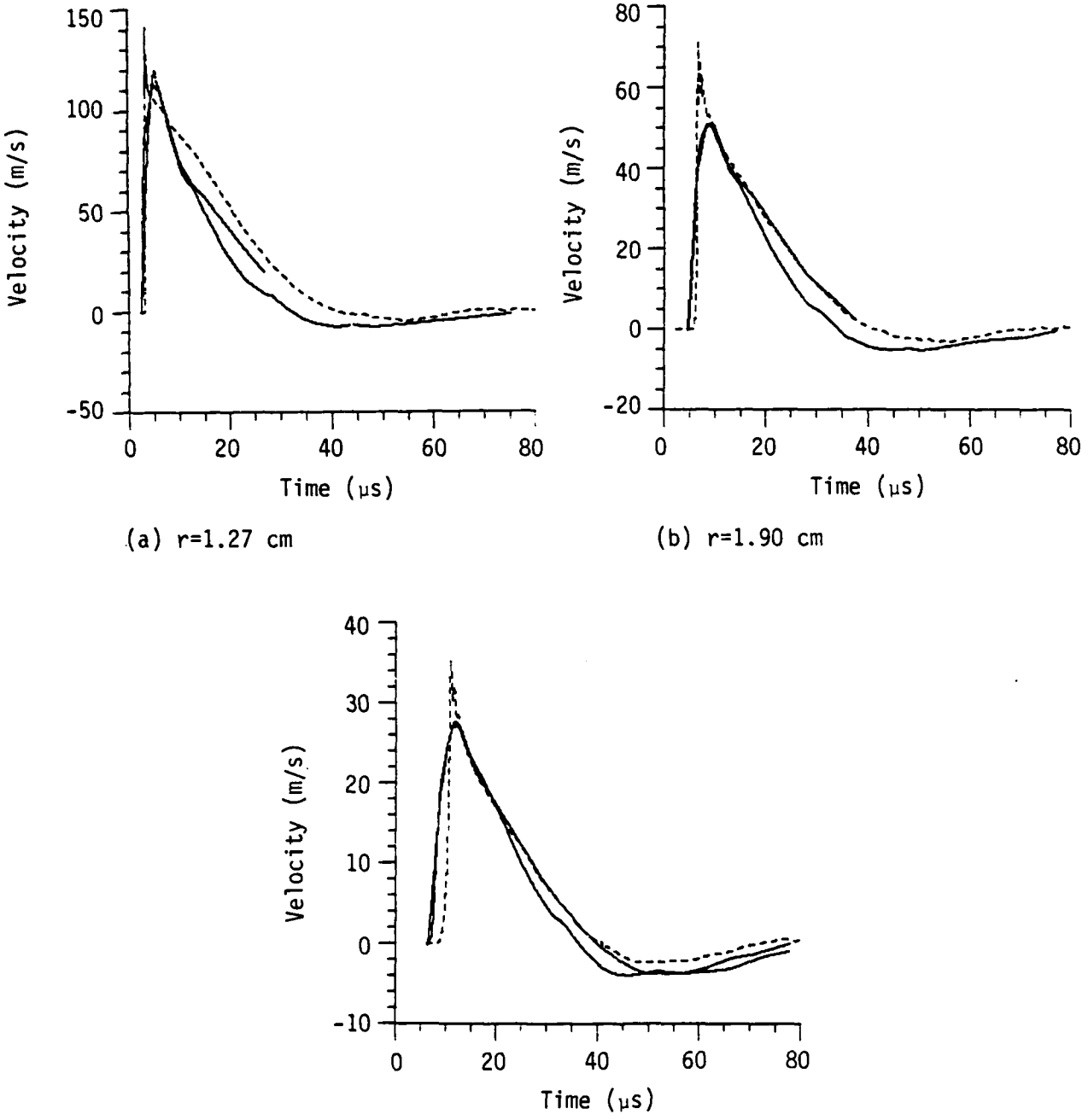


Figure 14. Comparison of SRI experiment data (solid) with calculation (dashed) using 2.2% air-void content and strain rate hardening on all the time.

strength while retaining agreement with the static lab tests. A comparison of the results with the experiment is shown in Figures 14 and 15. An air-void content of 2.2 percent was used. All the experimental traces were shifted roughly 2 microseconds in order to bring the time of arrival at the closest in stations into agreeement. This shift was necessary for all the model and SRI data comparisons shown.

There are several points to note concerning the results. Compared to the experiment, the calculation shows the wave speed associated with the first arrival to be slow, the rise times and peak to be sharper, and the attenuation rate of peak velocity to be too rapid. The duration of the computed outward motion, however, is now much closer to the measured one than the results shown in Figure 13.

Past experience with other Sandia HE tests in G-tunnel tuff has shown that the computed attenuation rate of the stress wave is too rapid when using the static measured air-void content.[8] The previous results show that this problem is also present in the SRI experiments. As discussed in Section 2, the baseline model was chosen to have an air-void content of 0.69% to allow for this expected bias in the measured air-void content. The results of a calculation using this model are shown in Figures 16 and 17. The attenuation rate and wave speed are now closer to the experimental results, but the signal is still quite late and low at the furthest station, and the sharp calculated rise time problem seen at the higher 2.2% air-void content is also present. Beyond the time of peak velocity, however, the agreement in overall wave shape between experiment and computation is seen to be quite good.

While there may be some reason to doubt the experimental traces, the reproducibility and quality of the SRI experiments has been such as to readily justify an effort to match the measured response. The philosophy adopted in this study was to consider the SRI data as a material property test and to then construct a material response model, biased but not constrained by the static lab measurements, that fit the measured velocity histories.

The model improvement procedure focused on the attenuation rate and rise time problems noted above. To keep the peak of the 8.0 cm station above 4 m/s it was necessary to completely eliminate the air-voids. A viscoelastic model (see Section 2.6)

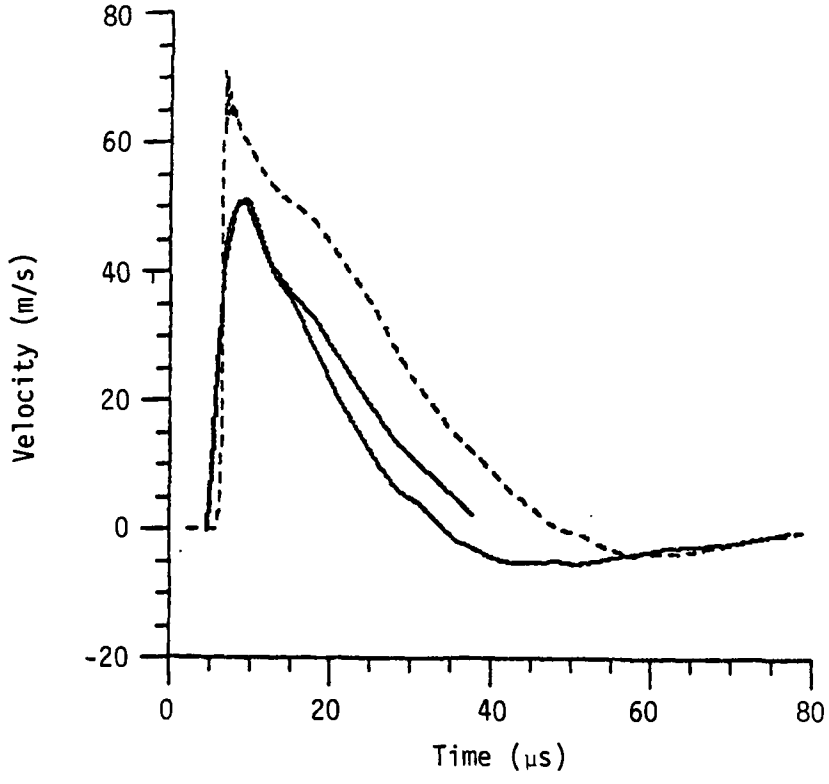


Figure 13. Comparison of SRI experiment data (solid) and calculation (dashed) at 1.90 cm location. The model used turned the strain rate hardening off upon damage.

## SECTION 3
## COMPARISON WITH SRI VELOCITY HISTORIES

This section compares calculated velocity histories with those obtained by SRI in their 3/8 gm PETN explosive tests in ONE-TON tuff. The first comparison is drawn between the SRI data and calculations using material response models that are consistent with the static Terra Tek data described in Section 2. These models did not do very well. Neither the attenuation rate of peak velocity nor the initial rise times matched the data. Following this comparison, a dynamic material response model that best matches these features is discussed and the improvement obtained is shown. This section ends with some conclusions and questions raised by these comparisons.

Any material response model constructed solely on the basis of the static data is not complete. In previous 3/8 gm explosive studies in 2C4 grout it was found that the yield strength required for a best match with SRI data had to be substantially increased over the static measured value[13]. This increase was ascribed to strain rate hardening. Such an effect is not unique to 2C4 grout; it has been seen in a variety of geologic materials. The additional issue of whether such hardening should be applied to the complicated damaged yield surfaces currently in use also must be addressed.

Some gas gun data exist which imply that a strain rate hardening of 30% per decade is appropriate for G-Tunnel tuff[14]. This hardening rate was included in the baseline model. In the absence of any further information, however, it was not clear whether to continue to apply this hardening once the material was damaged. The first calculation performed assumed that, like the successful 2C4 grout model[13], the strain rate hardening should be turned off on damage.

A comparison of this model calculation with experiment at the 1.90 cm location is shown in Figure 13. The major point to notice is the much longer duration of the positive phase of the motion shown by the calculation. This feature is common at all stations and results from a yield strength that is too weak after damage occurs.

The model for this tuff was changed so that the strain rate hardening applied to both the virgin and damaged strength. This was one way of increasing the damaged

The charge in the simulations of the SRI tests consisted of 0.3533 gm of PETN and 0.256 gm of lucite. Twenty cells of equal mass were used to model the PETN and sixteen equal mass cells were used for the lucite. This number of cells was necessary to allow the explosive model to come to the proper C-J state at the detonation front prior to reaching the surrounding tuff and lucite.

When the lucite was activated, 60 cells of tuff were added. The tuff zoning was radius matched to the last lucite cell and a sigma zoning scheme was used (i.e., the change in radius of each cell was increased by a constant 'sigma' geometric factor taken as 1.025 in this study). As the edge of the tuff region was activated the material behind the shock was rezoned two-for-one as necessary.

The ONE-TON charge consisted of 25 Kg of pentolite and 913 Kg of TNT. The explosive was finely zoned, with 20 equal mass cells in the Pentolite and 200 equal mass cells in the TNT. The TNT cells were mass matched to the Pentolite. In addition to the explosives, 70 cells of tuff were included. These cells were mass matched to the TNT and a sigma zoning scheme again was used, with sigma equal to 1.02. This scheme modeled the detonation and the coupling of the wave into the tuff as accurately as possible, within the limits of a reasonable number of zones.

Once the edge of the grid was activated in the ONE-TON computation the material behind the shock was rezoned five-for-one. All further rezones were two-for-one.

These strategies allowed the computations to be performed using very modest amounts of computer time and with sufficient resolution to model the shock front quite accurately. The artificial viscosity was chosen to have the smallest value consistent with very little overshoot and noise behind the shock front. The combination of small cells and artificial viscosity minimized numerical spreading of the shock front.

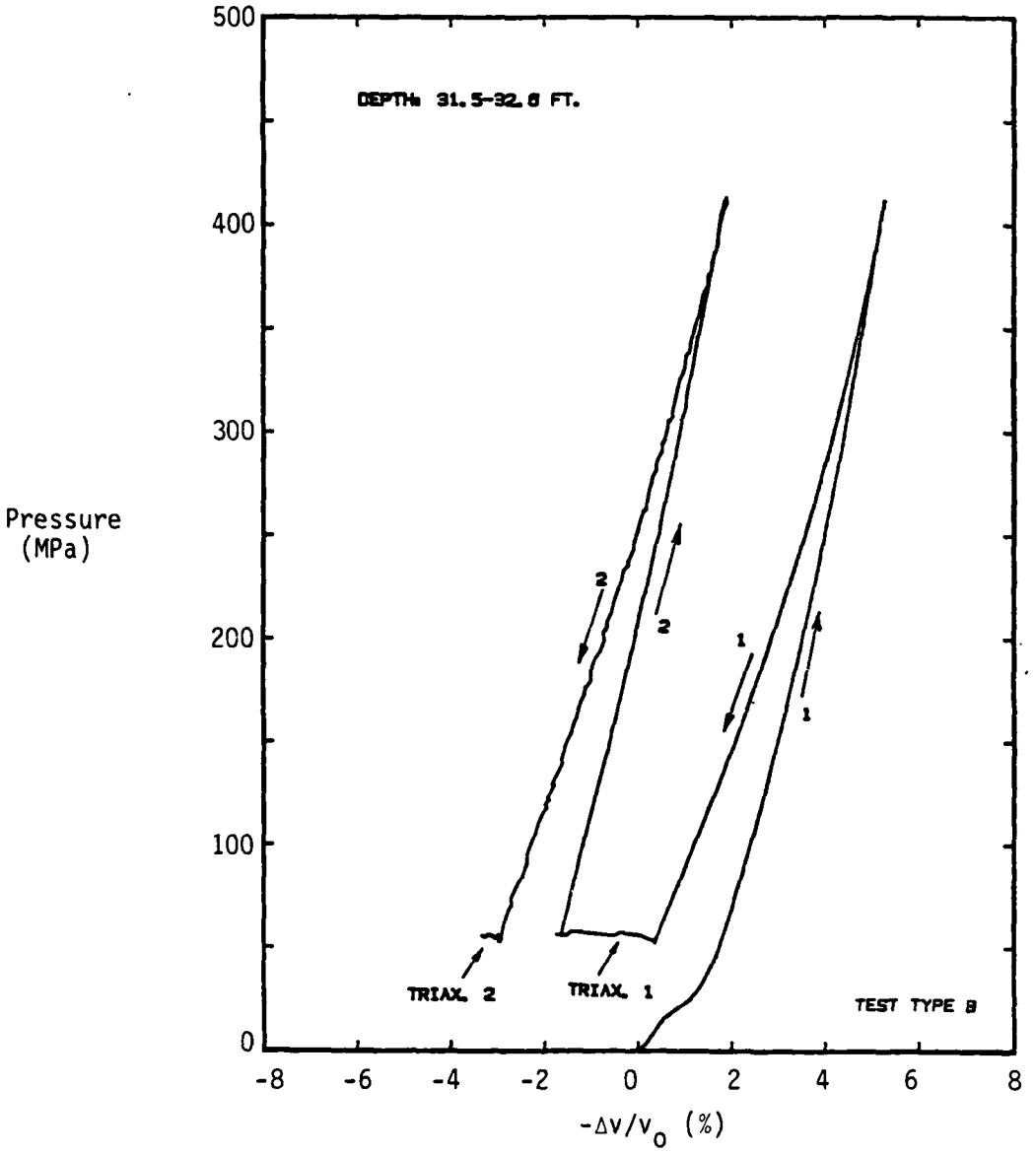


Figure 12. Typical Terra Tek U12G-OT tuff uniaxial load, biaxial unload, traixial loading data corresponding to the stress difference data shown in Figure 8.[2]

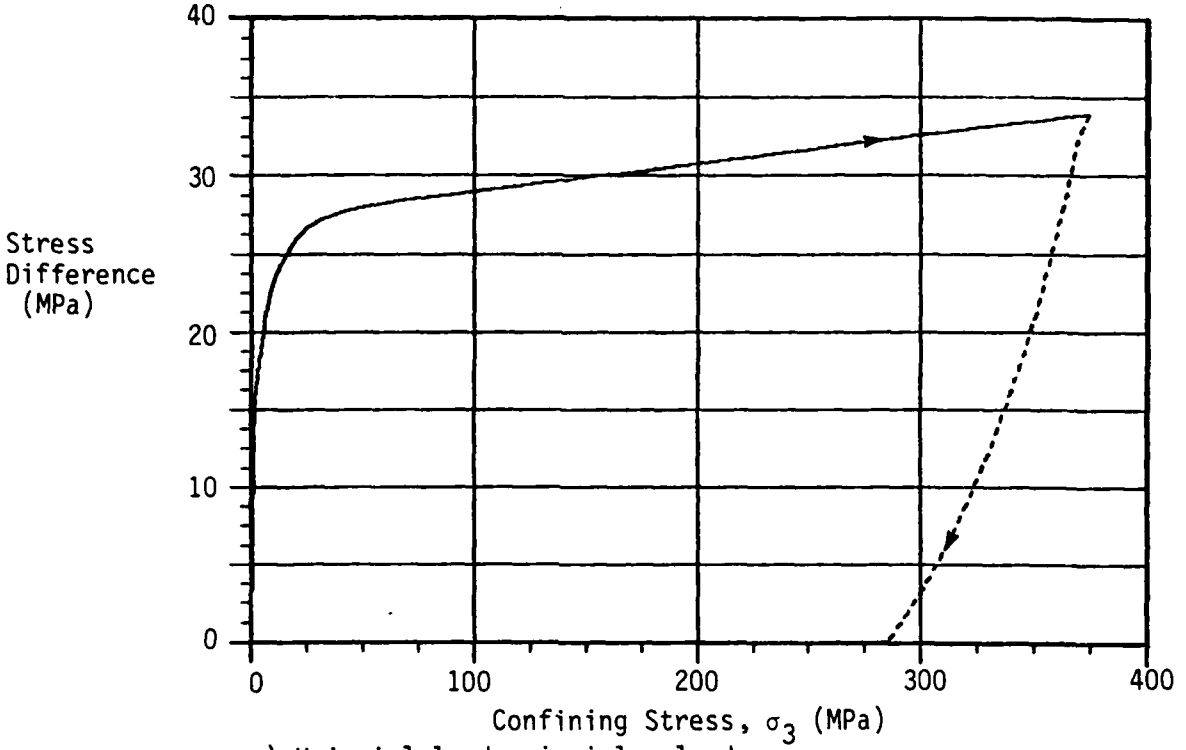


a) Uniaxial load-uniaxial unload

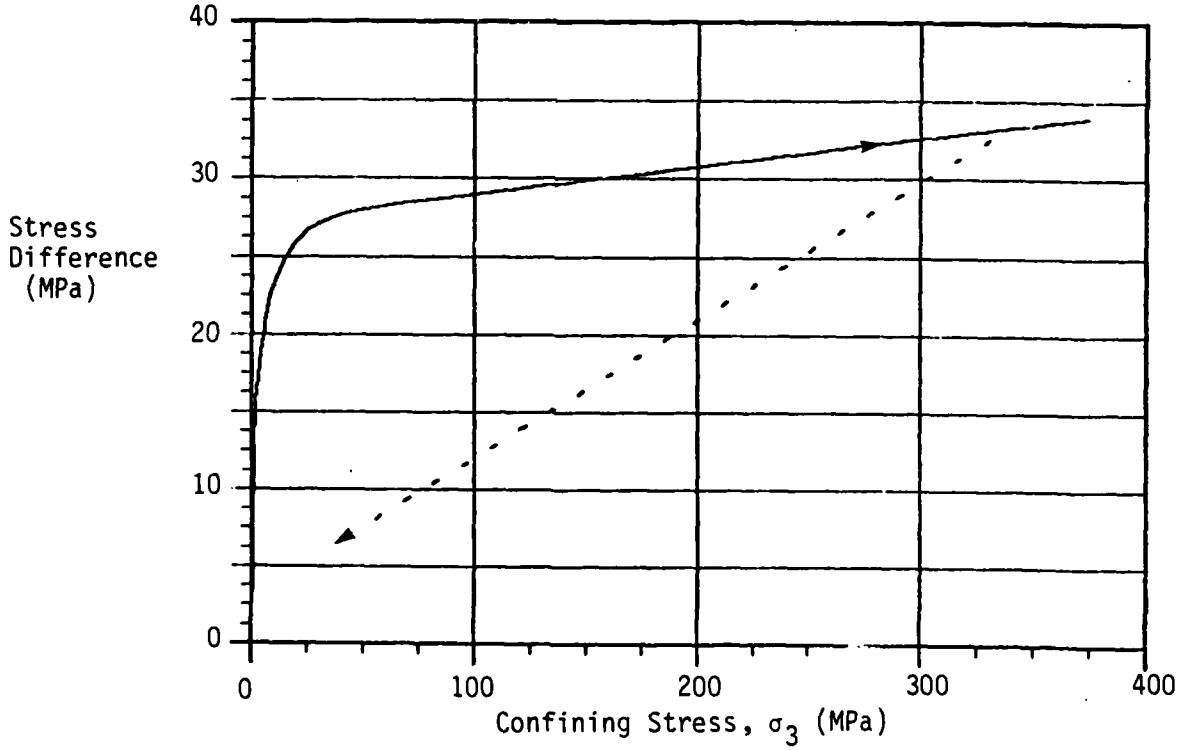


b) Uniaxial load-biaxial unload

Figure 11. Calculated stress difference vs. confining stress curves with dilatation model.

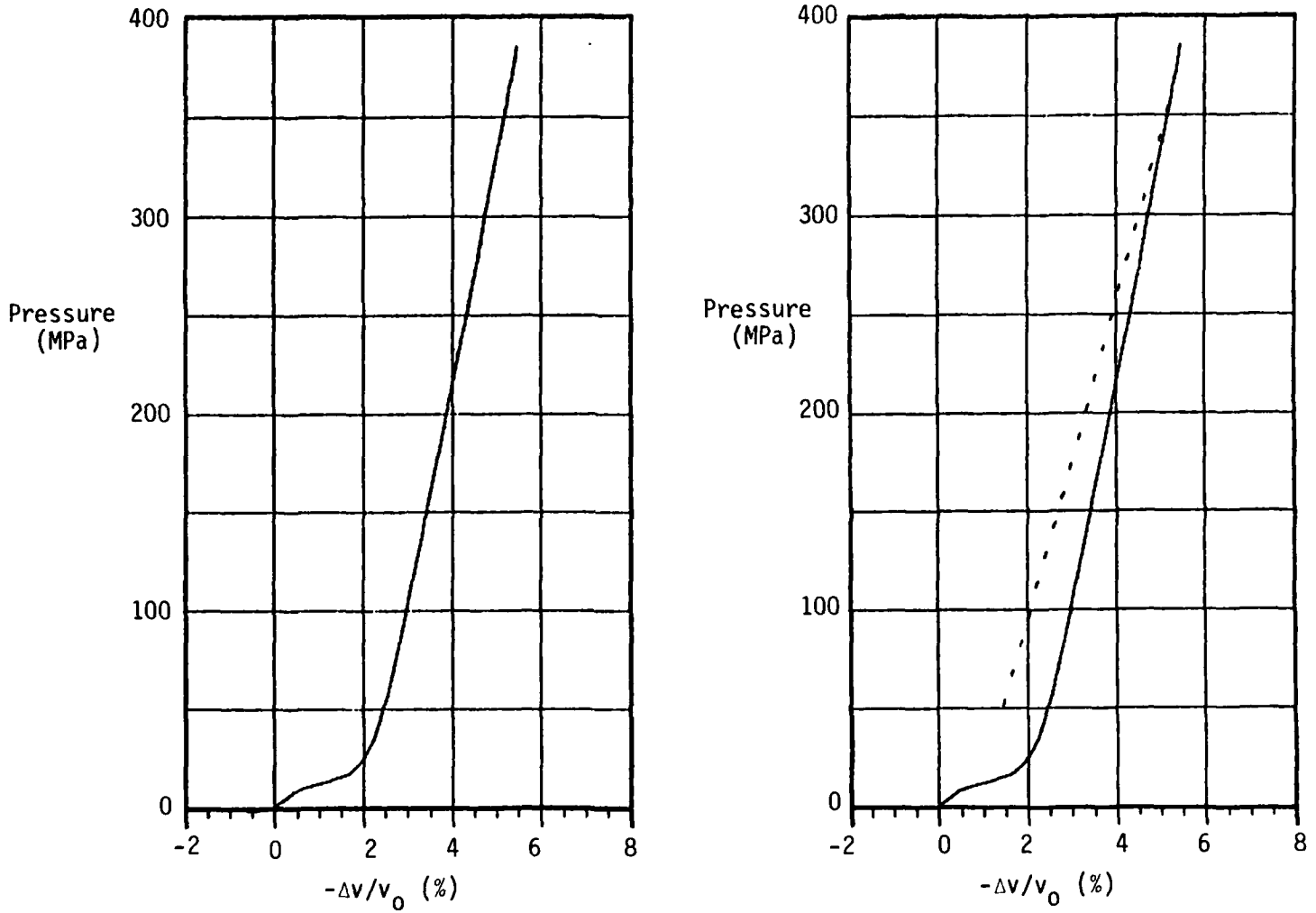


Figure 10. Calculated p-v load-unload response with dilatation model. Uniaxial unload in a) halted at 200 MPa when material hit the yield surface with $\sigma_1 < \sigma_3$.

above prescription. If the pressure is increased in the process of returning to the yield surface, then the material has undergone some dilation. Since both the volume and mass of material remains unchanged, the only way the pressure can be increased is for the rock matrix to be compressed to a higher density by the addition of air-voids.

The amount of dilatation induced in this process depends on the angle chosen for the line of return and the bulk modulus of the material. If the angle is too small and there is no restriction on the amount of air-voids added, it is possible to violate the Second Law of Thermodynamics. To avoid this problem a limit was placed on the total amount of air-voids created by this process.

Various angles of return and maximum dilatation were experimented with in the ONE-TON simulations. The results seemed insensitive to the total air-void content limit and a maximum of 6% was chosen as a reasonable value. The results were more sensitive to the angle chosen, however, as this determined the rate at which the tuff dilated in the calculation. The results shown below used an angle of 114 degrees.

Several calculations using the dilatation model were performed that simulated material properties tests in the laboratory. The results of a uniaxial strain loading test followed by a uniaxial strain unloading test are shown in Figures 10a and 11a. The corresponding Terra Tek results are shown in Figures 1 and 3. As can be seen, the calculated and measured stress-strain paths are in close agreement and no dilatation takes place. The results of a uniaxial load followed by a single biaxial unload are shown in Figures 10b and 11b with the Terra Tek results displayed in Figures 8 and 12. Again there is quite close agreement between the model results and experiment. Dilatation is clearly a factor in this test sequence.

## 2.8 CALCULATIONAL GEOMETRY AND PROCEDURE

The calculational procedure and grid were chosen to minimize the influence of artificial viscosity on the results. The strategy in the simulations of both the SRI and ONE-TON tests was to perform an explosive burn followed by an addition of the material driven by the explosive. The actual procedure differed slightly due to differences in the exposive charge used.

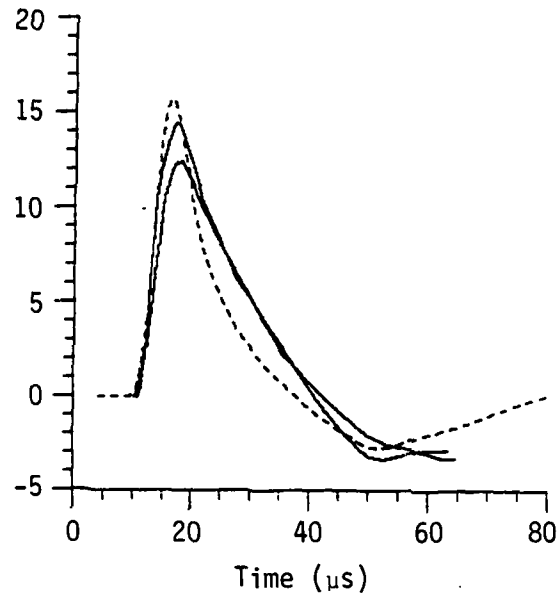


(a) r=4.0 cm

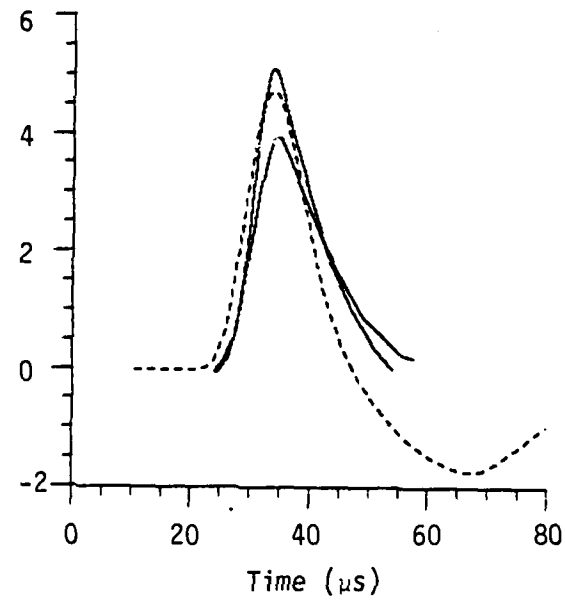


(b) r=8.0 cm

Figure 19. Comparison of SRI experiment data (solid) with a calculation (dashed) using a viscoelastic model and no air-void content.

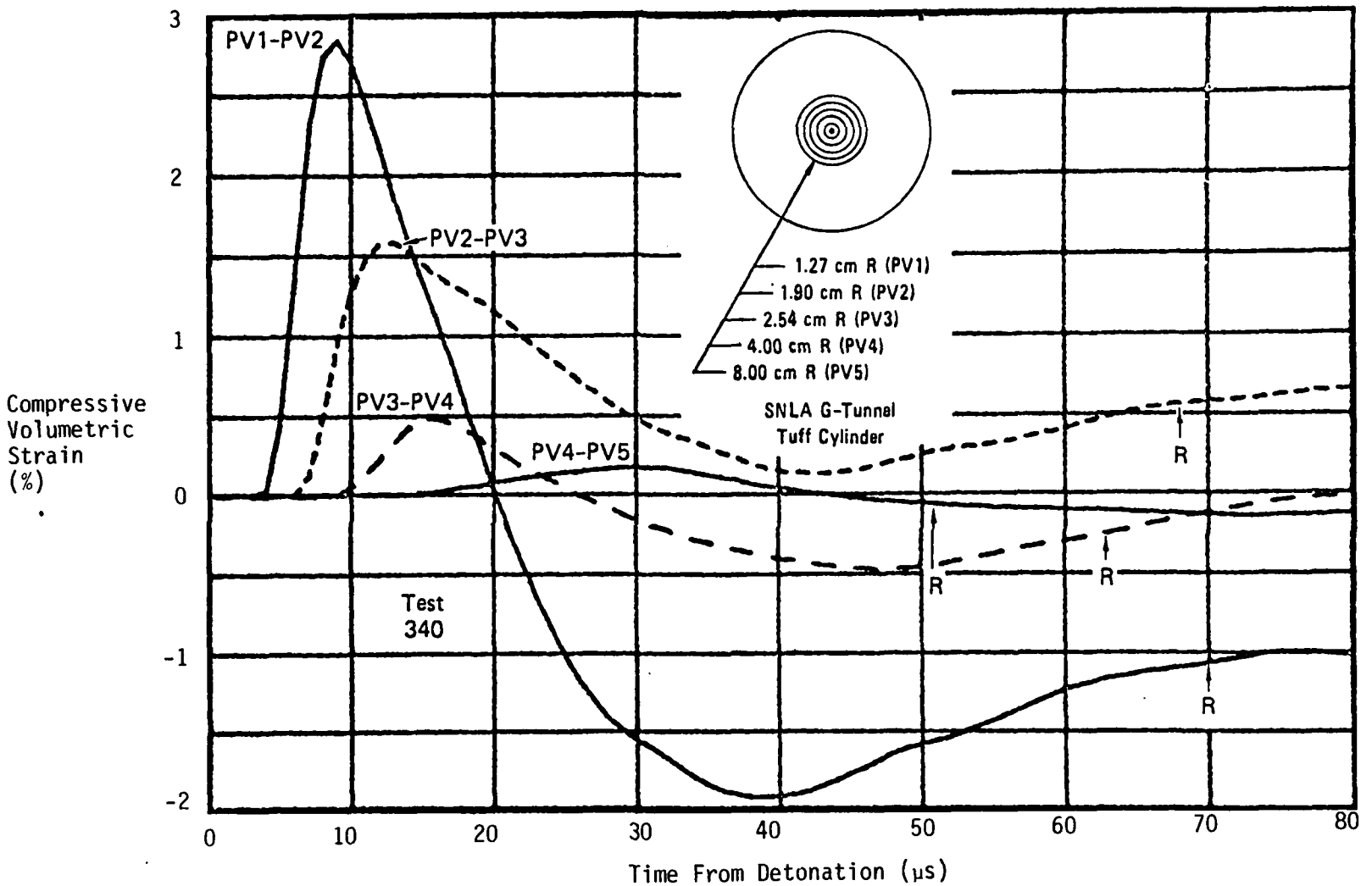


Figure 20. Volumetric strain measured by SRI by differencing particle velocity traces obtained in SNLA G-Tunnel tuff.

damaged strength observed in static material property tests. Whether the slow rise time and rounded character of the traces is due to some experimental problems associated with the grain size of the tuff or to an actual rate effect is also under investigation.

## SECTION 4
## COMPARISON WITH ONE-TON TEST DATA

This section deals with the comparison between the predictions and the experimental results of the Sandia ONE-TON test. All of the computations for ONE-TON were completed before the results of the field test were released. As such, the level of agreement achieved is indicative of the predictive capability of the present EOS modeling using static material property test data, both with and without the additional dynamic response information provided by the SRI test results. This section begins with a comparison of the prediction using the best material response model based solely on the static Terra Tek data and on past experience with small scale HE shots in G-Tunnel. Next, results from the model that produced the best match with the SRI results are presented. Finally, some conclusions are drawn based on these comparisons.

The comparison of the calculation using a response model based on static test data and the ONE-TON test data is indicated in Figures 21 through 24 in comparison to the ONE-TON test data. This tuff model used an assumed air-void content of 0.69% based on our past experiences in G-tunnel, and strain rate hardening was applied only to the strength of the undamaged material. Overall, the agreement is very good, even though this model performed quite poorly at the SRI scale as shown in Figure 13. On the SRI scale, this particular model produced a positive phase with a much longer duration than the experiment.

Based on the SRI results, strain rate hardening was applied to the strength of the damaged tuff as well as to the virgin material. A sample comparison of four closest stress gauges and the four velocity traces are shown in Figures 25 and 26. These comparisons are representative of results at more distant stations. Although this model change led to improvements in agreement on the SRI scale, the agreement on the ONE-TON scale is seen to be less satisfactory than that obtained with the original model. This implies that there is a definite rate effect in the response of this tuff that is not properly modeled by the simple percent per decade rule for strain rate hardening of the yield strength.

Comparisons between the viscoelastic model and the ONE-TON results are shown

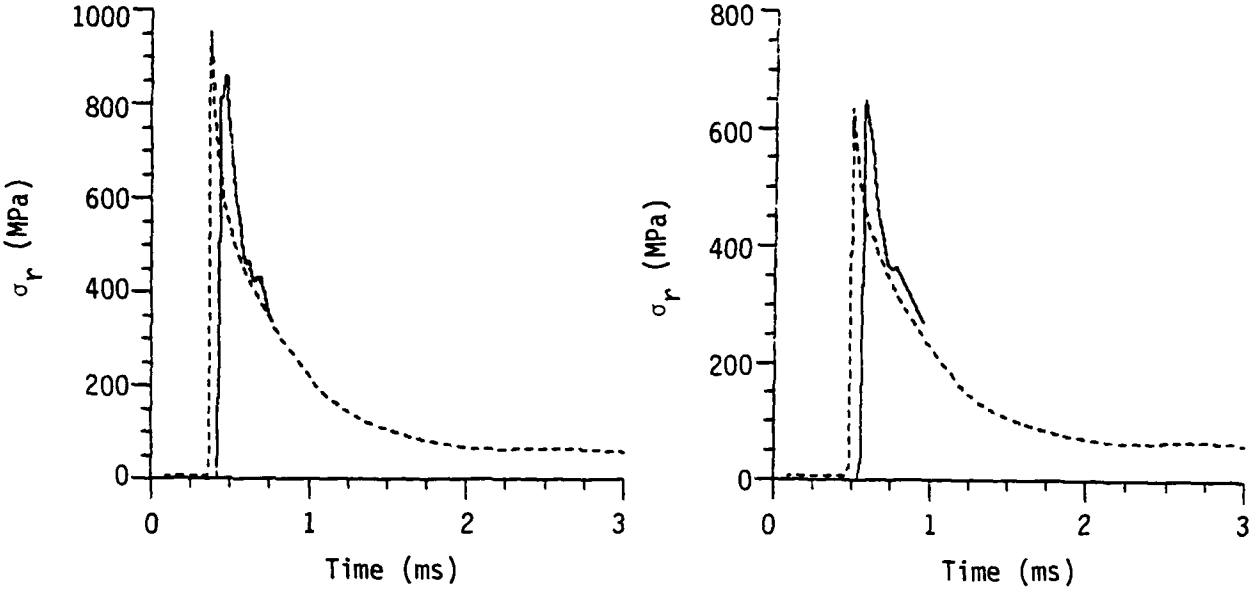


(a) Gauge 1YFC1, r=1.7m




(b) Gauge 2YFC1, r=2.03 cm

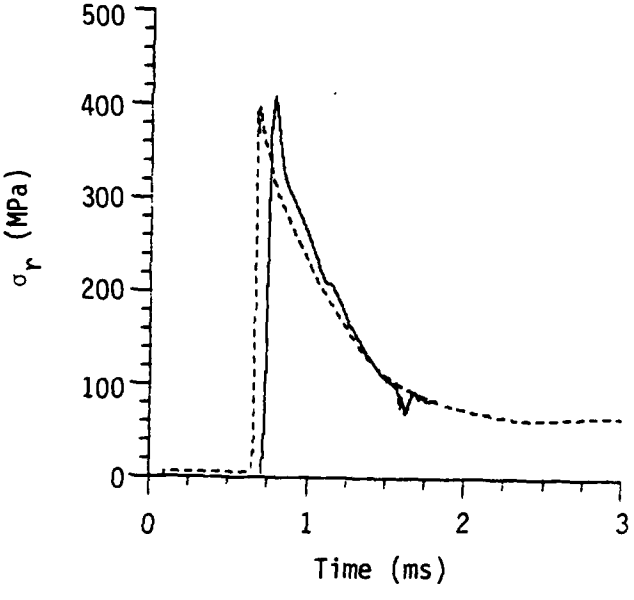


(c) Gauge 4YFC1, r=2.51 cm

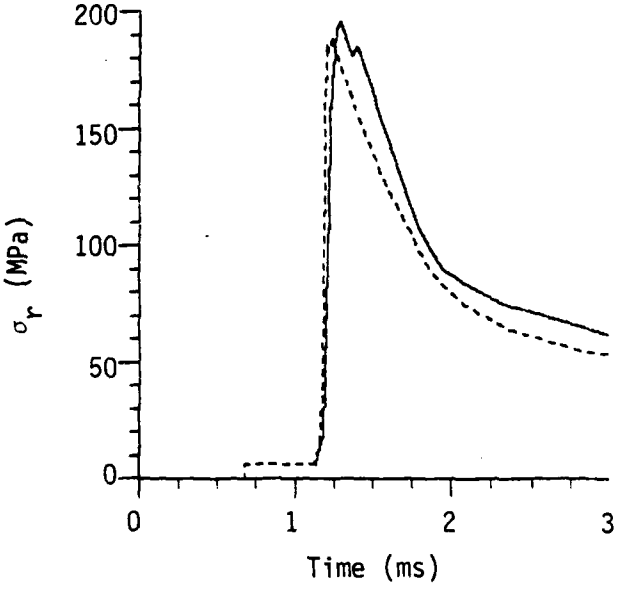


(d) Gauge 5YFC1, r=3.72 cm

Figure 21. Comparison of ONE-TON data (solid) with a calculation using the baseline static model with 0.69% air-void content.

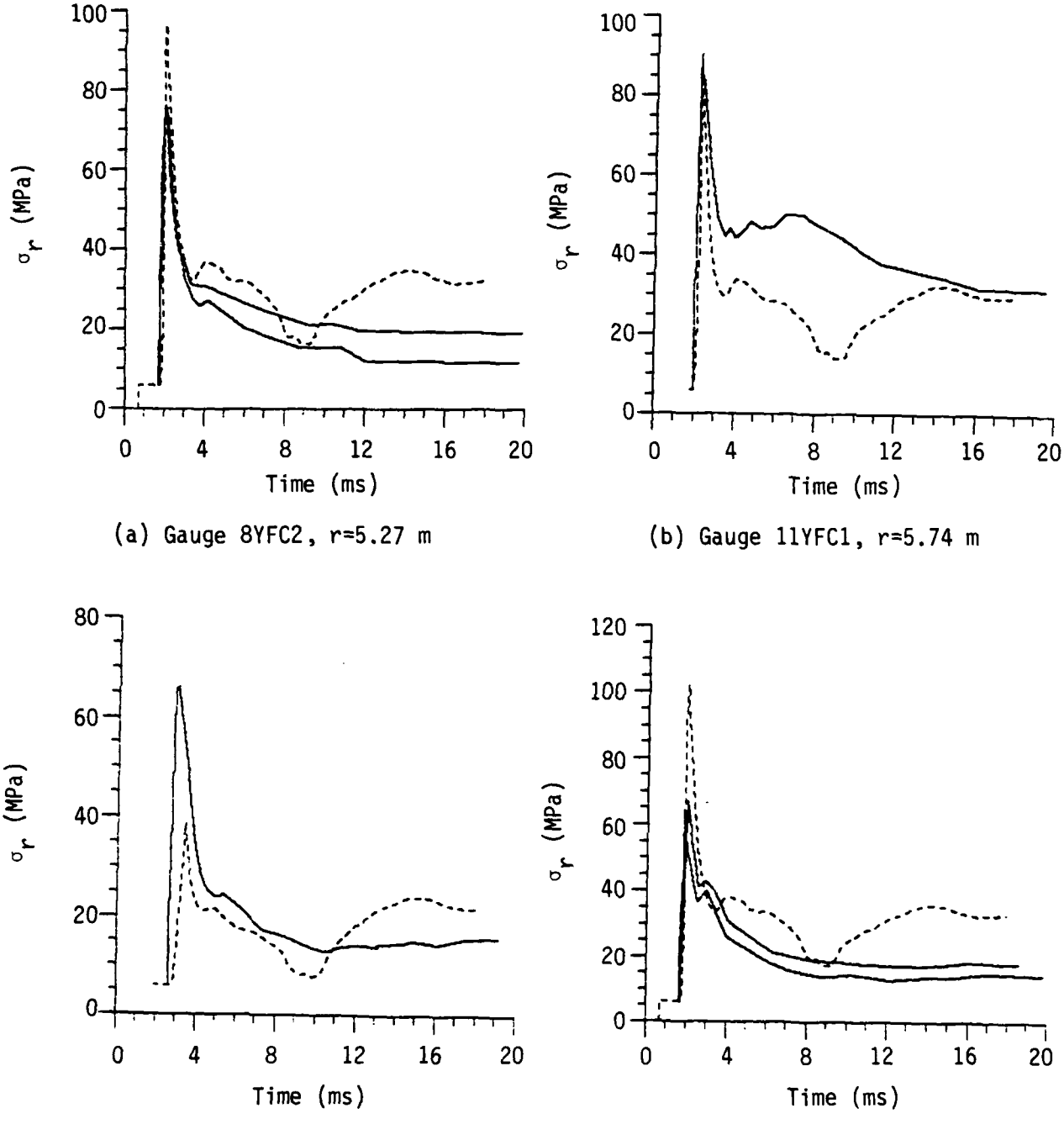


(a) Gauge 8YFC2, r=5.27 m

(b) Gauge 11YFC1, r=5.74 m

(c) Gauge 12YPC1, r=7.63 m

(d) Gauge 9TS1, r=5.16 m

Figure 22. Comparison of ONE-TON data (solid) with a calculation using the baseline static model with 0.69% air-void content.

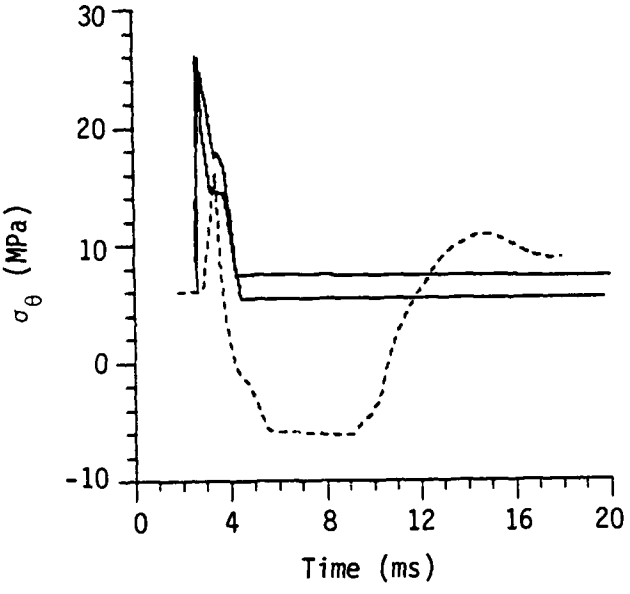


(a) Gauge 9PC2, r=7.60 m

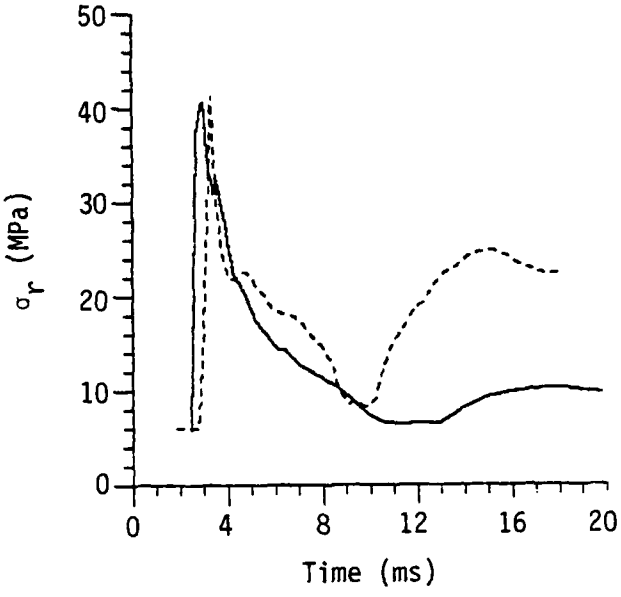


(b) Gauge 9TS2, r=7.45 m

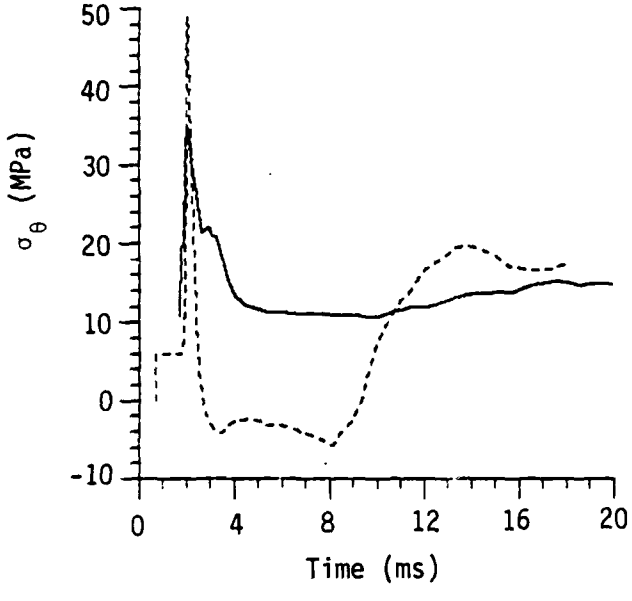


(c) Gauge 9PC1, r=5.32 m

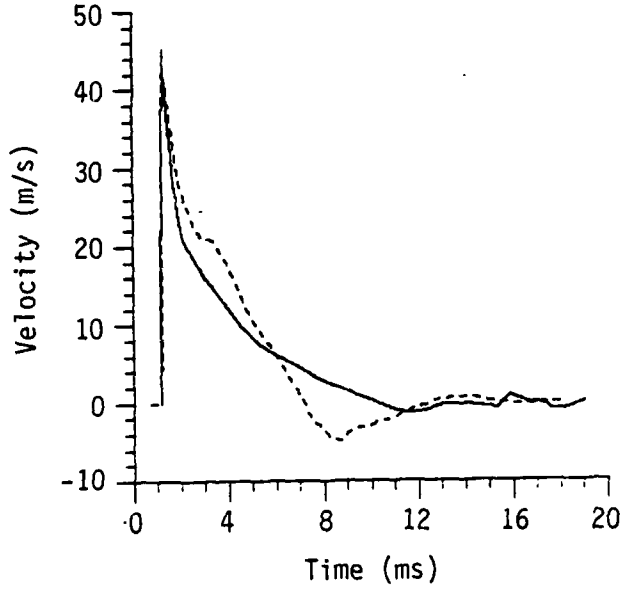


(d) Gauge 5AC1, r=3.72 m

Figure 23. Comparison of ONE-TON data (solid) with a calculation (dashed) using the baseline static model with 0.69% air-void content.

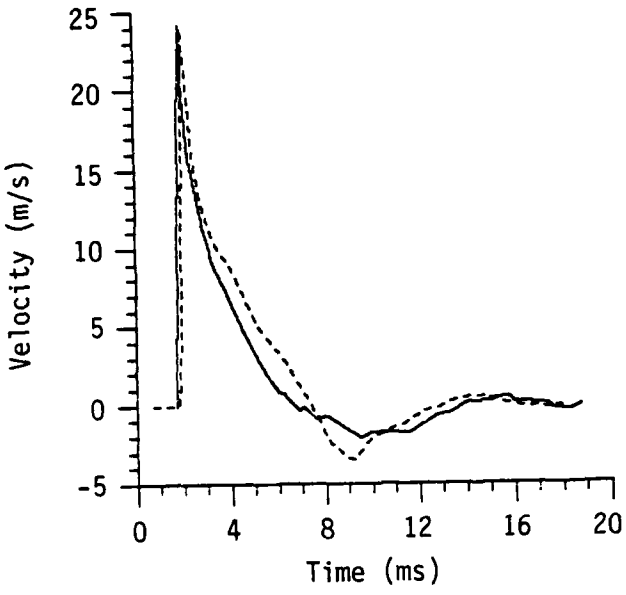


(a) Gauge 8AC1, r=5.27 m

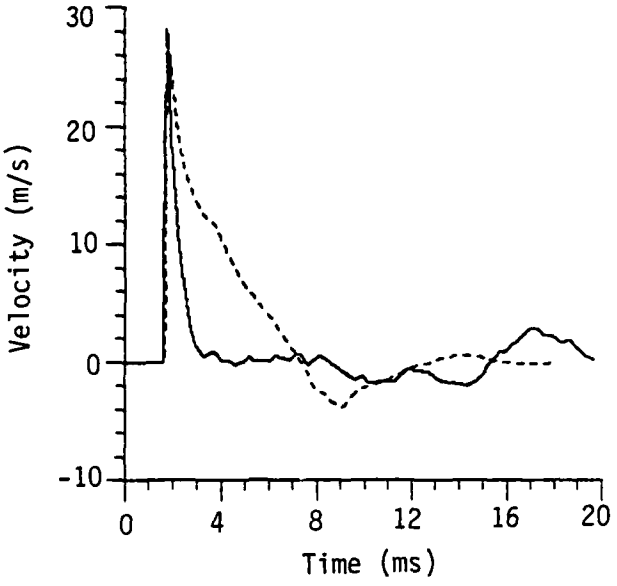


(b) Gauge 10AC1, r=4.83 m

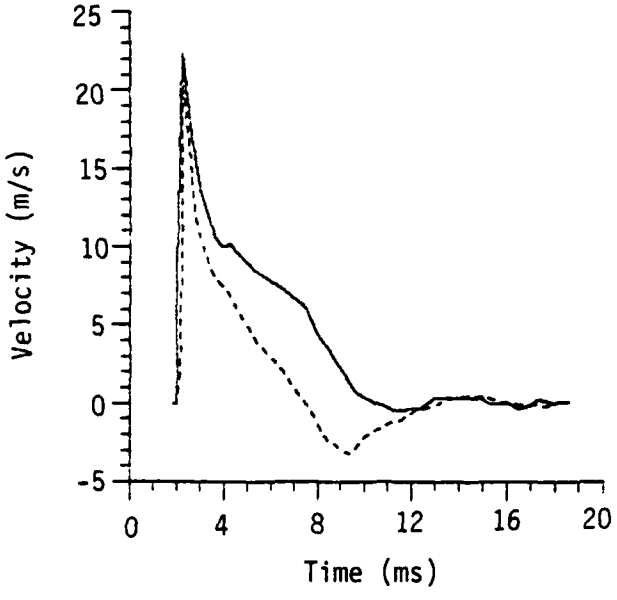


(c) Gauge 11AC1, r=5.73 m

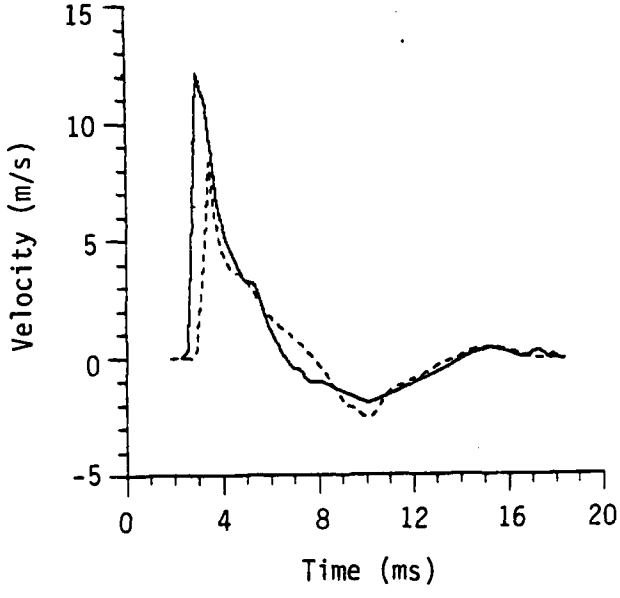


(d) Gauge 12AC1, r=7.63 m

Figure 24. Comparison of ONE-TON data (solid) with a calculation (dashed) using the baseline static model with 0.69% air-void content.

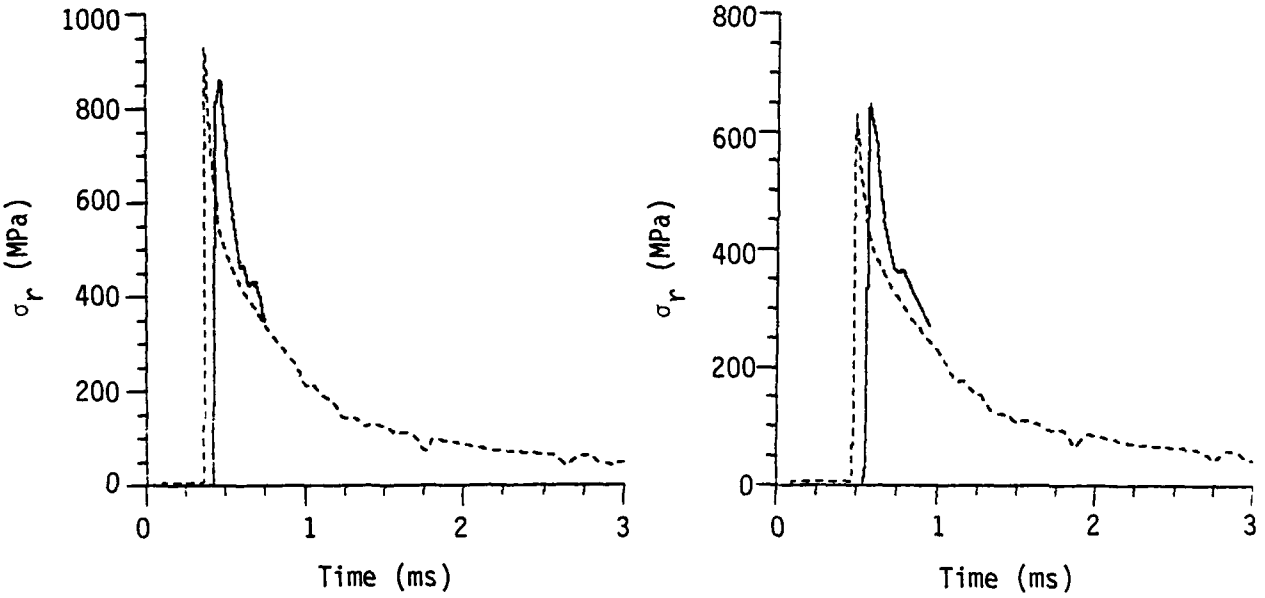


(a) Gauge 1YFC1, r=1.70 m




(b) Gauge 2YFC1, r=2.03 m

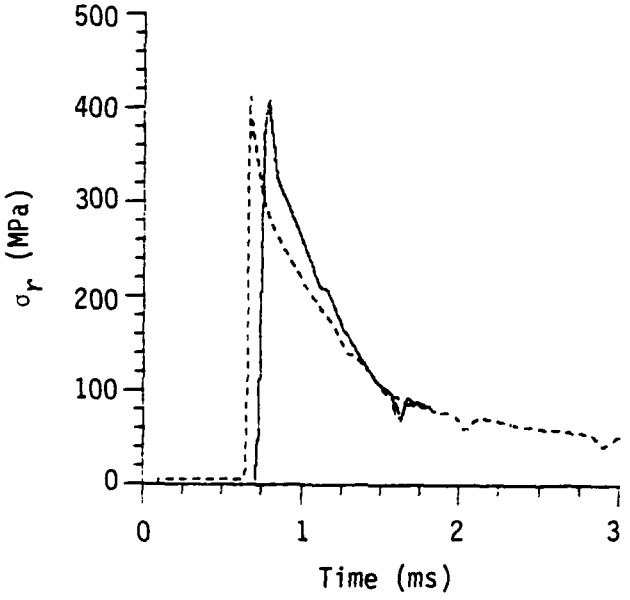


(c) Gauge 4YFC1, r=2.51 m

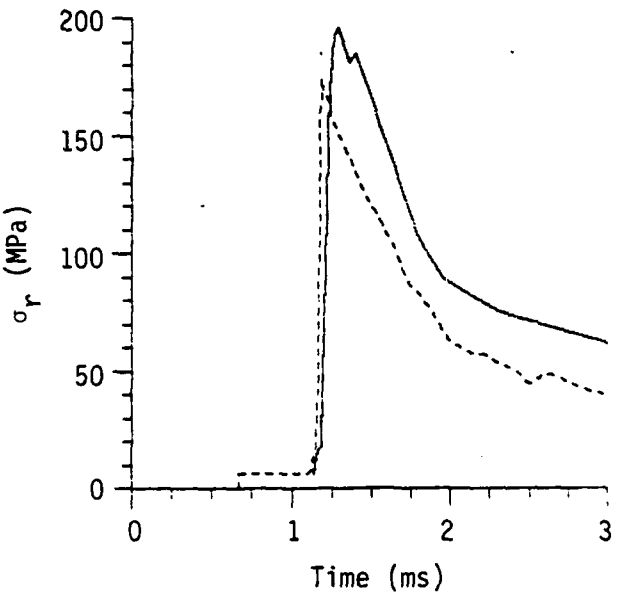


(d) Gauge 5YFC1, r=3.72 m

Figure 25. Comparison of ONE-TON data (solid) with a calculation (dashed) using 0.69% air-void content and strain rate hardening on after damage.

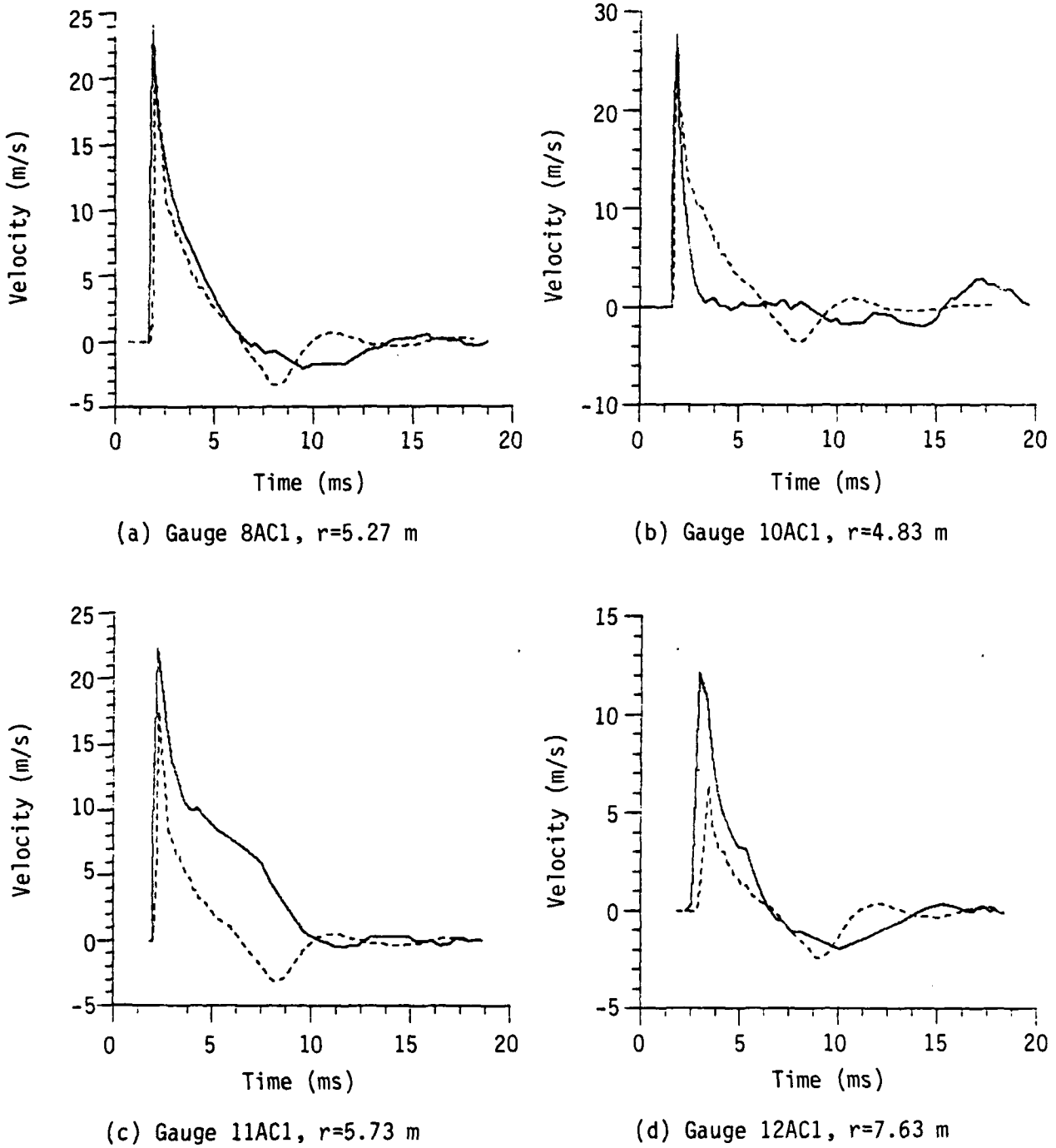


Figure 26. Comparison of ONE-TON data (solid) with a calculation (dashed) using 0.69% air-void content and strain rate hardening on after damage.

in Figures 27 through 30. The agreement is quite good. In fact, in our judgment the viscoelastic model appears to give slightly better overall results than the baseline model (shown in Figures 21 to 24). The reader is invited to decide which he prefers by a careful comparison of the two sets of results. Important features to note in making these comparisons are that the peak attenuation of stress in the viscoelastic model is somewhat less than the baseline model, while arrival times for the viscoelastic model are nearly perfect. These observations are not too surprising since the moduli in the viscoelastic model were determined using the wavespeeds seen in the SRI experiments, and the absence of air-voids accounts for the lower attenuation rate in the viscoelastic model.

The ONE-TON results again focus attention on the issue of strain rate dependence. The viscoelastic model includes a rate effect in the bulk modulus, and this relatively simple model produces very good agreement with both the SRI and ONE-TON results. It accommodates the pulse duration and arrival times seen at both scales. Its major deficiency is that it does not extrapolate back to the static measured response.

The problem of reconciling the measured attenuation rates with the air-void content has been repeatedly mentioned. A preliminary attempt was made to accommodate the measured air-void content without inducing excessive attenuation by using a dilation model. This explanation was suggested by the measured dilatancy seen in the static tests as well as being inferred from the SRI velocity records as discussed in Section 3. The trial dilatation model used an non-associated flow rule to dictate the degree of dilatancy. The angle of return to the yield surface was dictated by the rapidity with which the volume expansion was required and, in general, was not normal to the yield surface.

A comparison of results from this dilatancy model with the ONE-TON data is shown in Figures 31 and 32. These results are representative of all the stations. The wave pulses are a bit too broad and the attenuation is only postponed out to the 80 Mpa peak stress range. Beyond that range there is a very rapid attenuation not seen in the data. These are preliminary results, and work along this line is ongoing.

In summary, once the air-void content was reduced in the calculational model, both

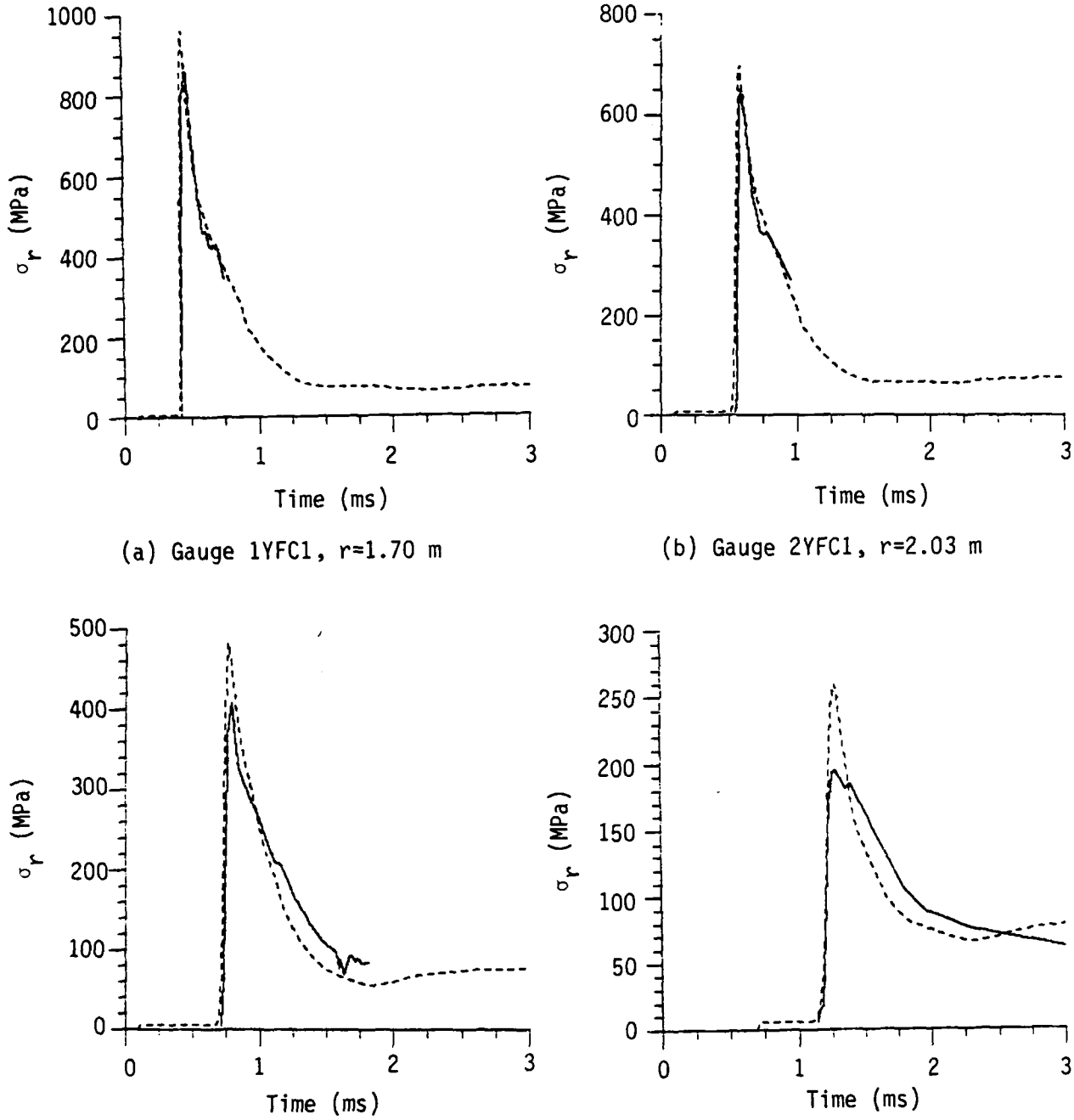


(a) Gauge 1YFC1, r=1.70 m

(b) Gauge 2YFC1, r=2.03 m

(c) Gauge 4YFC1, r=2.51 m

(d) Gauge 5YFC1, r=3.72 m

Figure 27. Comparison of ONE-TON data (solid) with a calculation (dashed) using the viscoelastic model.

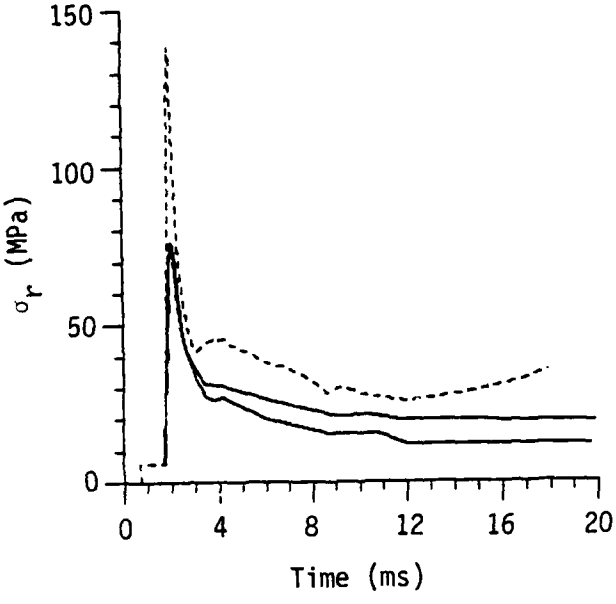


(a) Gauge 8YFC2, r=5.27 m

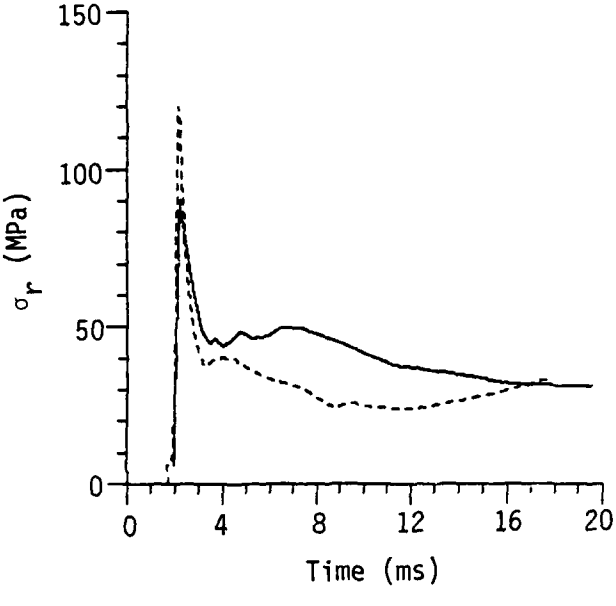


(b) Gauge 11YFC1, r=5.74 m

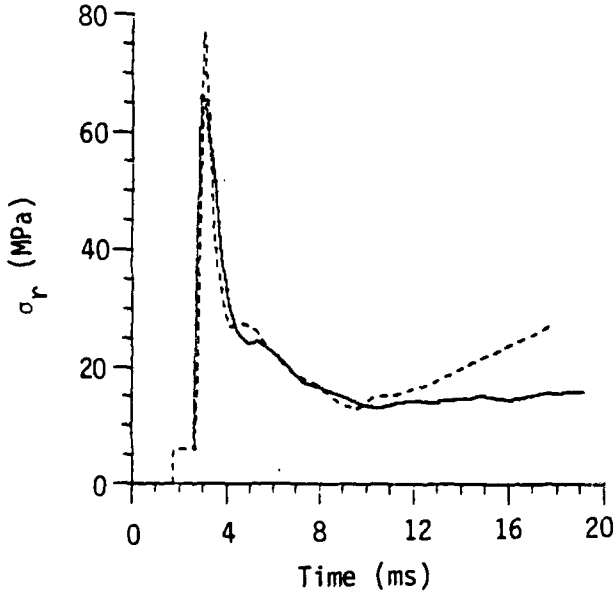


(c) Gauge 12YFC1, r=7.63 m

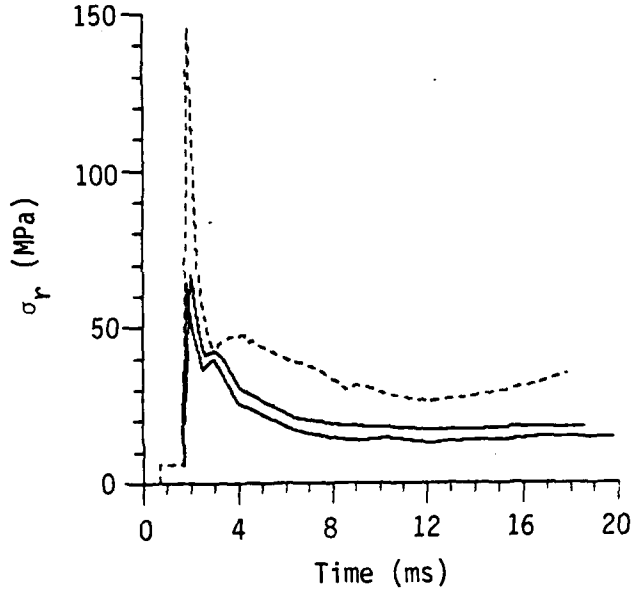


(d) Gauge 9TS1, r=5.16 m

Figure 28. Comparison of ONE-TON data (solid) with a calculation (dashed) using the viscoelastic model.

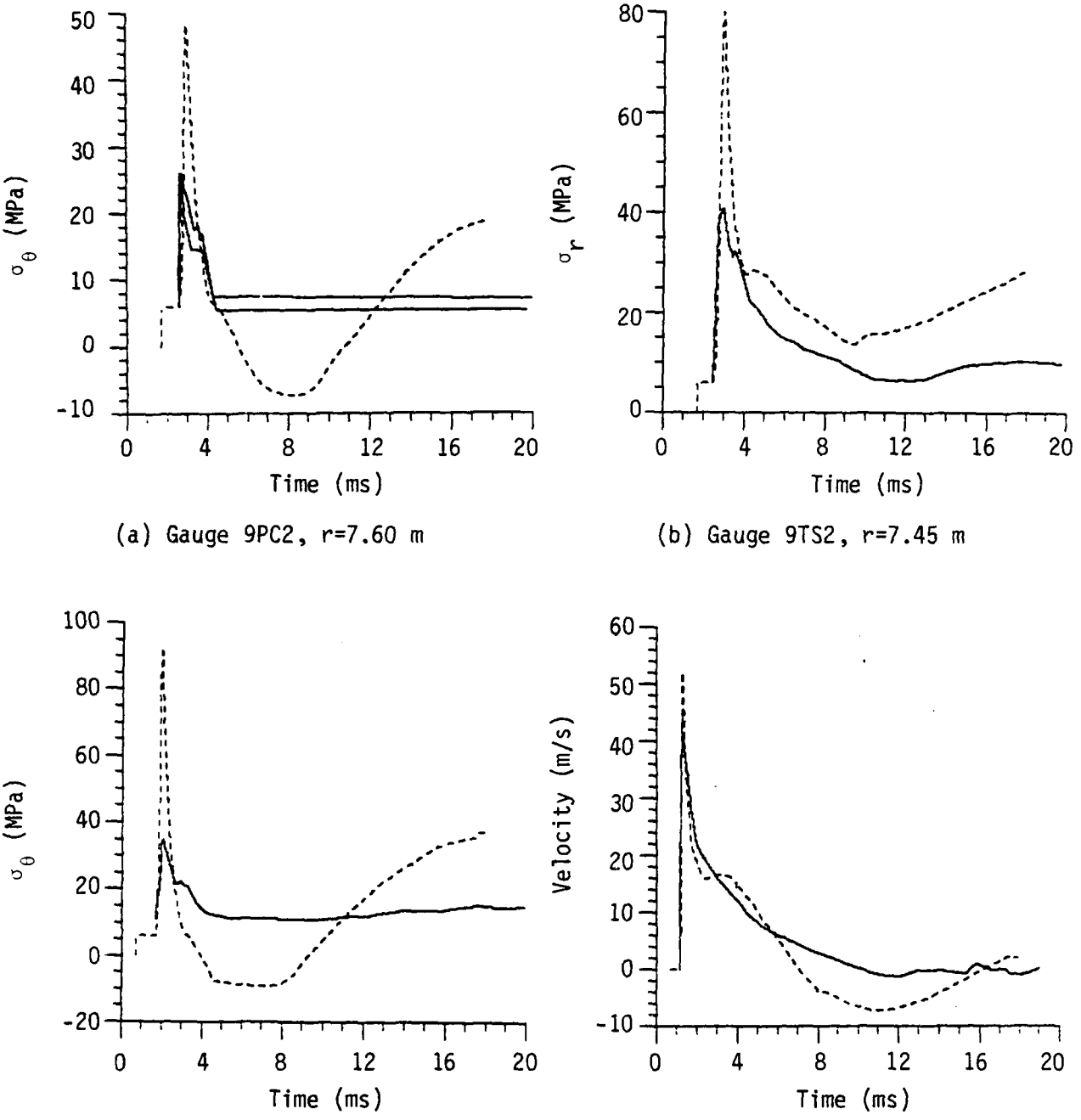


(a) Gauge 9PC2, r=7.60 m

(b) Gauge 9TS2, r=7.45 m

(c) Gauge 9PC1, r=5.32 m

(d) Gauge 5AC1, r=3.72 m

Figure 29. Comparison of ONE-TON data (solid) with a calculation (dashed) using the viscoelastic model.

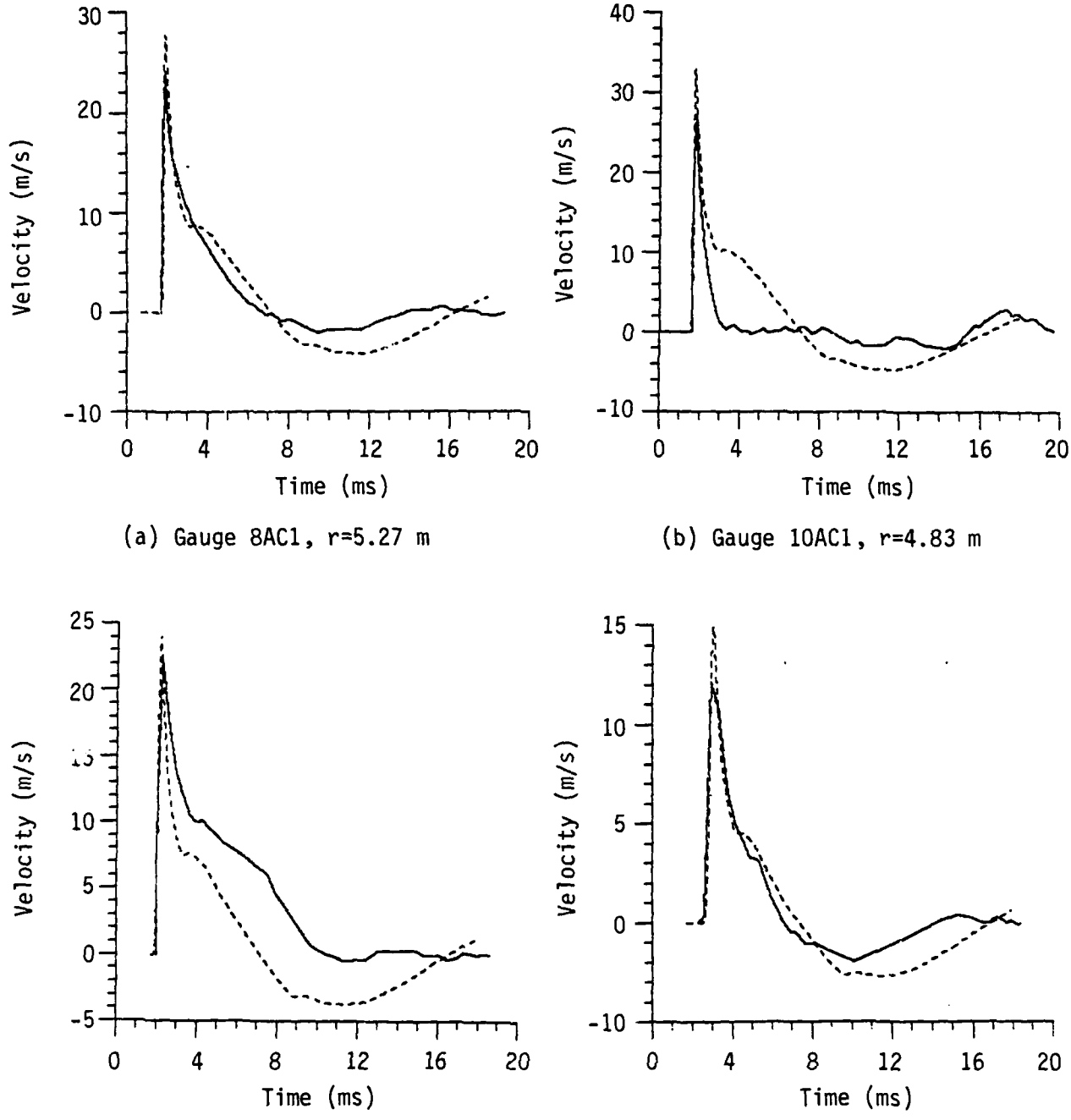


(a) Gauge 8AC1, r=5.27 m

(b) Gauge 10AC1, r=4.83 m

(c) Gauge 11AC1, r=5.73 m

(d) Gauge 12AC1, r=7.63 m

Figure 30. Comparison of ONE-TON data (solid) with a calculation (dashed) using the viscoelastic model.

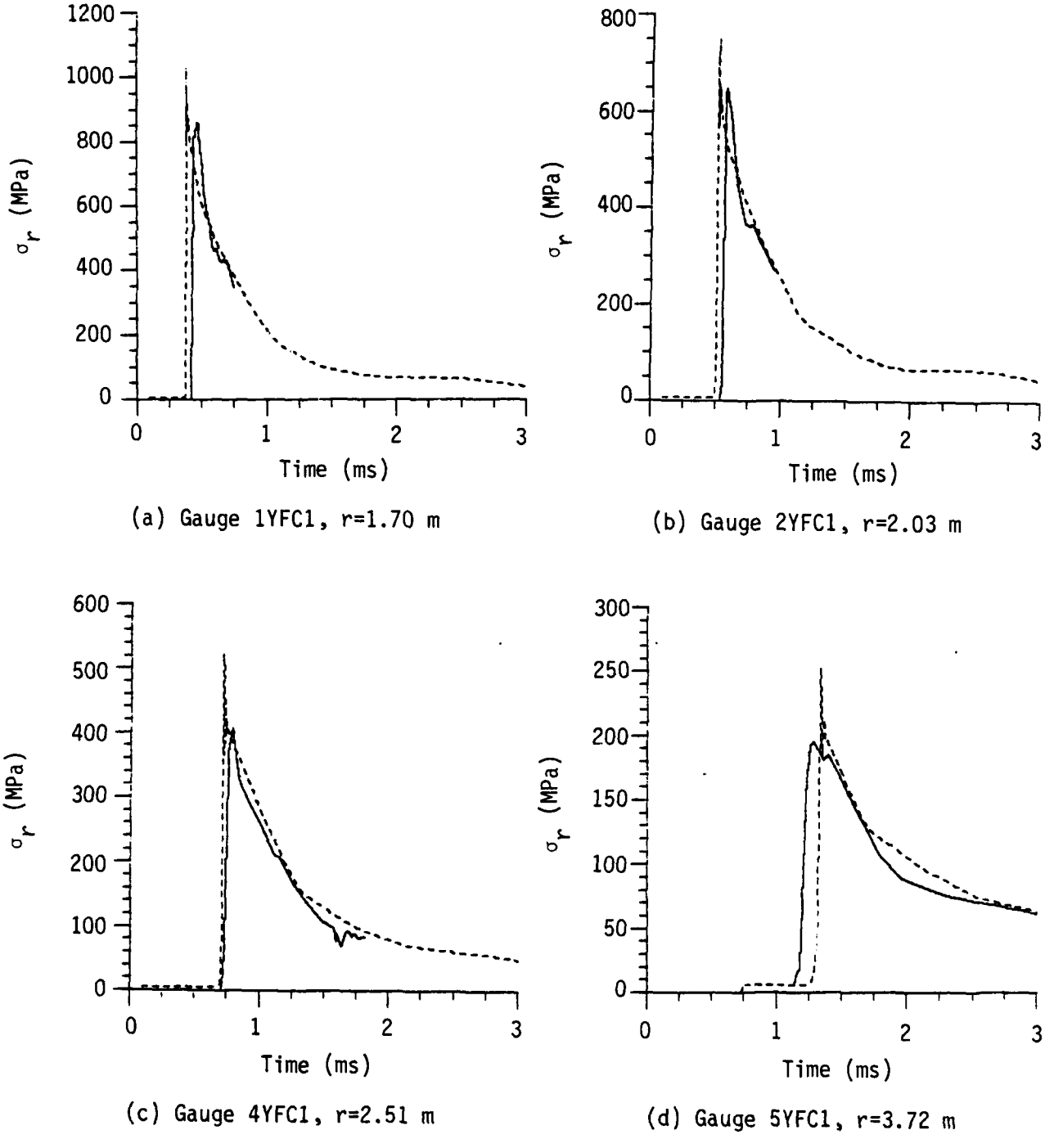


(a) Gauge 1YFC1, r=1.70 m

(b) Gauge 2YFC1, r=2.03 m

(c) Gauge 4YFC1, r=2.51 m

(d) Gauge 5YFC1, r=3.72 m

Figure 31. Comparison of ONE-TON data (solid) with a calculation (dashed) using a model with 2.2% air-void content and dilatancy.

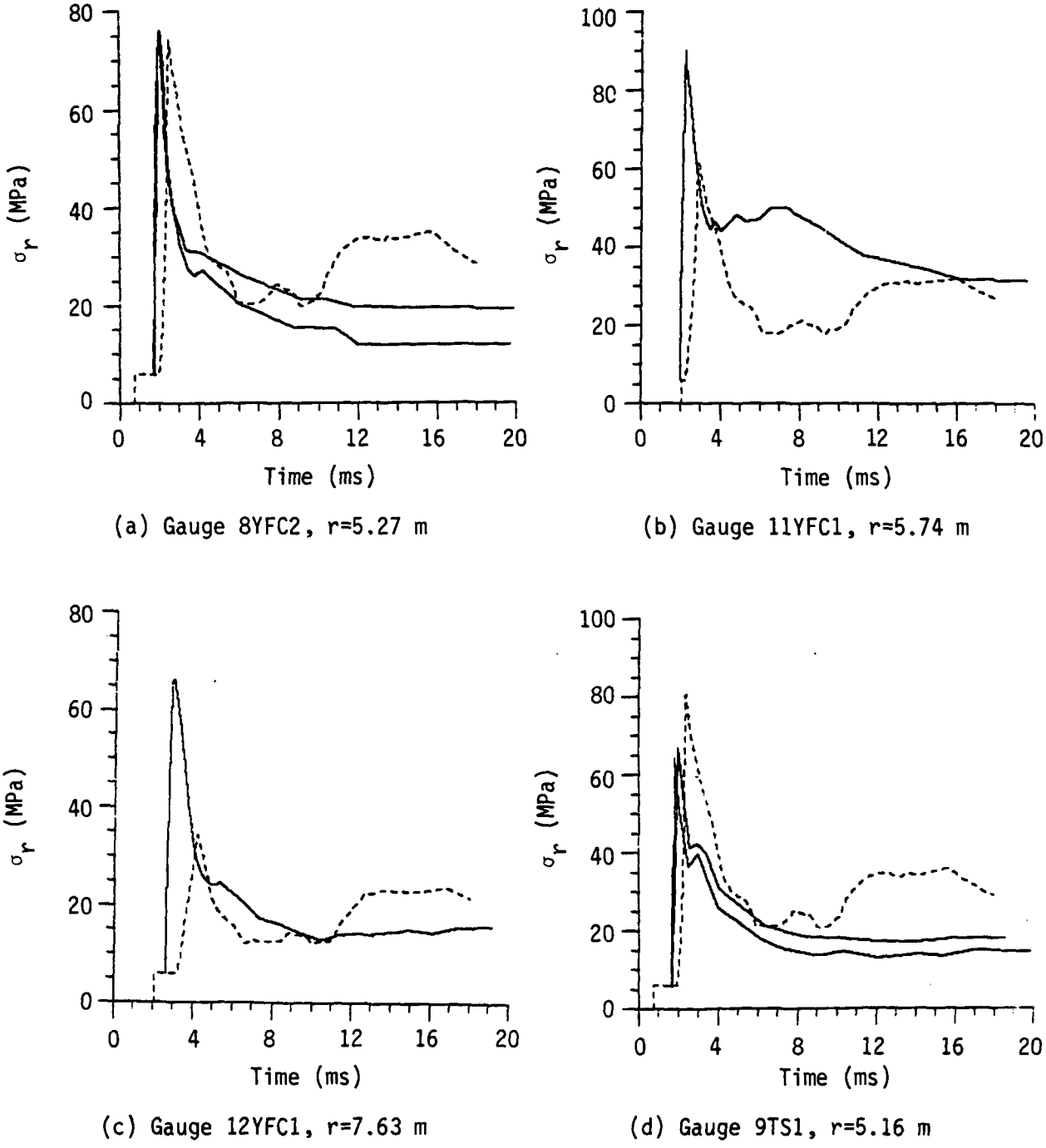


(a) Gauge 8YFC2, r=5.27 m

(b) Gauge 11YFC1, r=5.74 m

(c) Gauge 12YFC1, r=7.63 m

(d) Gauge 9TS1, r=5.16 m

Figure 32. Comparison of ONE-TON data (solid) with a calculation (dashed) using a model with 2.2% air-void content and dilatancy.

the model constructed as a best fit to the remainder of the static test data and the model that fit the SRI response did quite well in matching the ONE-TON results. These comparisons show quite clearly the presence of rate effects in the material response, and no one model has succeeded in spanning the measured response from the static regime to the high strain rates experienced at the SRI scale. The issue of insitu or effective air-void content is present in both the ONE-TON and SRI tests. Work to date suggests that it will be difficult to reconcile the measured 2.2% air-void content with the peak attenuation rate of either stress or velocity as seen in the explosive tests with the present dilatation model.

## SECTION 5
## SUMMARY AND CONCLUSIONS

The major purpose of the research discussed in this report was to identify the strengths and weaknesses of current EOS modeling techniques. To accomplish this objective without bias the comparisons proceeded in a blind fashion, i.e., the predictions were reported before the experimental results were released. Comparisons at two scales were carried out and the correlation of those results and the calculations led to several useful conclusions and questions. These issues will be summarized in this section.

A series of lab tests were performed by Terra Tek to help in the construction of an equation of state for G-Tunnel tuff. These tests included standard hydrostatic, uniaxial, and triaxial test sequences. In addition to these familiar test sequences, cycled tests such as uniaxial load - biaxial unload, and multiple, uniaxial load - unload tests were performed. These relatively unorthodox measurements were very useful in developing the static response model, particularily in including the nature of the damaged strength. Considerable evidence of dilatancy was found, but this aspect of the tuff behavior was not included in any of the conventional material models considered because a number of outstanding questions remained about the details of an appropriate formulation for this difficult aspect of the constitutive model.

Traditionally, material response models used in explosive earth motion computations have been developed using material properties measured under essentially static test conditions. Such a procedure clearly is inherently risky, but has proved successful for a variety of materials (even at the high strain rates of the SRI scale) provided minor adjustments are made to account for differences between the measured bulk modulus and ultrasonic wavespeeds.

The first clear evidence that static properties might not be sufficient to define the response of tuff at the SRI scale was the unexpectedly small measured cavity size for explosions in 2 C4 grout. This observation implied that the static strength measured for 2 C4 grout was too low under the dynamic conditions of the SRI test. To increase the dynamic yield strength of the grout without being inconsistent with the static value, a simple strain rate dependent model was invoked to increase the dynamic yield strength.

Such an effect has been observed in gas gun experiments on some geologic materials. With appropriate values for the strain rate strength increase, excellent agreement was obtained between measured and computed cavity size and velocity histories for 2 C4 and LD2 C4 grouts. Very small cavity sizes subsequently were also observed on the SRI shots in the ONE-TON tuff.

The experimental data imply a rather important strain rate effect in going from the ONE-TON to SRI scale, if the SRI data are taken at face value. This is emphasized by the comparisons of calculations done using the same model and the two sets of experimental results. It was shown that it is possible to extrapolate the static model to the ONE-TON scale, but not all the way to the SRI scale. It was also possible to accommodate both the SRI and ONE-TON data with one model. No model, however, was able to span the complete range in rate from static to the SRI scale. The demonstrated presence of this strong strain rate effect points out the hazzards inherent in using data taken at one or two widely separate rates to develop a general purpose material model expected to cover a wide range of stress-strain space.

The success of the viscoelastic model appears to be especially interesting. This model was constructed using only the SRI data, in particular, the first and peak arrival times of the velocity traces. As pointed out by Allen[16], the first arrival wave speed for SRI is 3160 m/s and the peak arrival speed is 2480 m/s, while the first arrival wave speed for the ONE-TON test is 2700 m/s. The difference of the wavespeeds at these two scales is clear evidence of a nontrivial strain rate effect operating on the moduli and is accommodated quite well by the viscoelastic model.

The second issue highlighted by the above comparisons is the inconsistency beween the measured air-void content and attenuation rate of peak stress and velocity. Calculations using the measured air-void content of 2.2% showed much too much attenuation. Best agreement was obtained using an air-void content below 0.7%. This is consistent with past experience in G-Tunnel.

The air-void issue is complicated by the dilatant behavior measured in physical property tests and inferred from the velocity records at the SRI scale. First attempts to incorporate this feature of the tuff response in a model with 2.2% air-void content led to

some improvement in the attenuation rate. The wave shapes, however, were not in very good agreement with the data. Clearly, this subject requires further work.

With the above considerations taken as qualifications, rather good agreement was obtained between predictions and the experiment at the ONE-TON scale. This agreement demonstrates that the current models are adequate to faithfully reproduce material response provided the appropriate constants in the models can be specified. With the exception of the air-void content question currently being studied, and the need for at least a simple strain rate dependent strength model, static test data are suitable for modeling any field event of reasonable scale. Resolution of the remaining questions should help to further improve the models currently in use.

## REFERENCES


1. Smith, C. W., "ONE-TON Experiment Data," presented at ONE-TON Experimental Review Meeting at S-Cubed, 14 October 1983.

2. Private communications from C. H. Cooley, Terra Tek, Joseph LaComb, Defense Nuclear Agency, 25 May, 24 August and 23 September 1983.

3. Cizek, J. C. and Florence, A. L., "Laboratory Investigation of Containment of Underground Explosions," SRI International Bimonthly Progress Report No. 2, April 1983.

4. Cooley, C. H., Terra Tek, letter to Joseph LaComb, Defense Nuclear Agency, 28 February 1983.

5. Private communication from Craig Cooley, Terra Tek, to Dan Patch, Pacifica Technology, of U12G.0T 24 Hour Creep - Uniaxial Strain Data, 2 December 1983.

6. Ellis, W. L. and Ege, J. R., "Determination of In Situ Stress in U12g Tunnel, Rainier Mesa, Nevada Test Site, Nevada," U.S. Geological Survey, USGS-474-219, January 1976.

7. Patch, D. F., M. B. Fogel and R. T. Allen, "Underground Nuclear Test Stemming and Containment Studies (U)," Pacifica Technology Final Report, PT-C83-0634, 4 November 1983.

8. Patch, D. F., "Results from Low Yield Test Design Calculations," Pacifica Technology Technical Note, PT-U81-0519, 16 September 1981.

9. Patch, D. F., M. B. Fogel and R. T. Allen, "Underground Nuclear Test Stemming and Containment Studies (U)," Pacifica Technology Final Report, PT-C83-0634, 4 November 1983.

10. Patch, D. F., Pacifica Technology, presented at the DNA Ground Motion Calculators Meeting at S-Cubed, 14 April 1981.

11. Butters, S. W., et al, "Material Properties of Nevada Test Site Tuff and Grout - with Emphasis on the DIABLO HAWK and HYBLA GOLD Events," Defense Nuclear Agency Final Report, DNA 4528F, November 1977.

12. Cooley, C. H., Smith, R. H. and Schatz, J. F., "Properties of Tuffs, Grouts and Other Materials - Final Report for Period September 1979 to November 1981," Terra Tek, TR 82-05, January 1982.

13. Fogel, M. B. and Patch, D. F., "Deviatoric Response Models and Residual Stress Field Calculations for SRI Grout," Pacifica Technology Report, PT-U83-0591, 13 January 1983.

14. Private communication from Carl Smith, Sandia, to M. B. Fogel, Pacifica Technology.

15. Cizek, J. C. and Florence, A. L., "Laboratory Investigation of Containment of Underground Explosions," SRI International Draft Final Report, December 1983.

16. Allen, R. T., Pacifica Technology, letter to Carl Keller, Defense Nuclear Agency, 2 November 1983.

# DISTRIBUTION LIST

DEPARTMENT OF DEFENSE

Defense Nuclear Agency
ATTN: SPTD, T. Kennedy
4 cys ATTN: STTI-CA

Defense Tech Info Center
12 cys ATTN: DD

Field Command, Defense Nuclear Agency
ATTN: FCTT, W. Summa
ATTN: FCT, Col G. Ballantine
3 cys ATTN: FCTK, C. Keller
3 cys ATTN: FCTK, E. Rinehart

DEPARTMENT OF ENERGY

Department of Energy
Nevada Operations Office
ATTN: P. Mudra

OTHER GOVERNMENT AGENCY

US Geological Survey
ATTN: R. Carroll
ATTN: P. Orkild

DEPARTMENT OF ENERGY CONTRACTORS

Desert Research Institute
ATTN: D. Schulke Sec Off for P. Fenske
ATTN: D. Schulke Sec Off for C. Case

University of California
Lawrence Livermore National Lab
ATTN: L-209, G. Higgins
ATTN: R. Terhune
ATTN: F. Morrison
ATTN: L. Makague
ATTN: B. Hudson
ATTN: C. Olsen

Los Alamos National Laboratory
ATTN: R. Brownlee
ATTN: C. Keller
ATTN: F. App
ATTN: T. Kunkle, ESS-5
ATTN: B. Travis

DEPARTMENT OF ENERGY CONTRACTORS (Continued)

Sandia National Laboratories
ATTN: Org 7112, C. Mehl
ATTN: R. Bass
ATTN: C. Smith

DEPARTMENT OF DEFENSE CONTRACTORS

California Research & Technology, Inc
ATTN: M. Rosenblatt

Kaman Tempo
ATTN: DASIAC

Kaman Tempo
ATTN: DASIAC

Pacific-Sierra Research Corp
ATTN: H. Brode, Chairman SAGE

Pacifica Technology
2 cys ATTN: D. Patch
2 cys ATTN: M. Fogel

Physics International Co
ATTN: J. Shea
ATTN: H. Wampler
ATTN: J. Gordon

R&D Associates
ATTN: P. Haas

Rand Corp
ATTN: B. Bennett

S-CUBED
ATTN: C. Dismukes
ATTN: R. Duff

SRI International
ATTN: A. Florence

END

FILMED

5-85

DTIC